AD-A037 103 WORCESTER POLYTECHNIC INST MASS DEPT OF PHYSICS F/G 20/5
NON-LINEAR OPTICAL AMPLIFICATION AND ABSORPTION.(U)
FEB 77 L M NARDUCCI DAAG29-76-G-0075
UNCLASSIFIED ARO-13603.1-R-P NL

1 OF 1
ADA037103

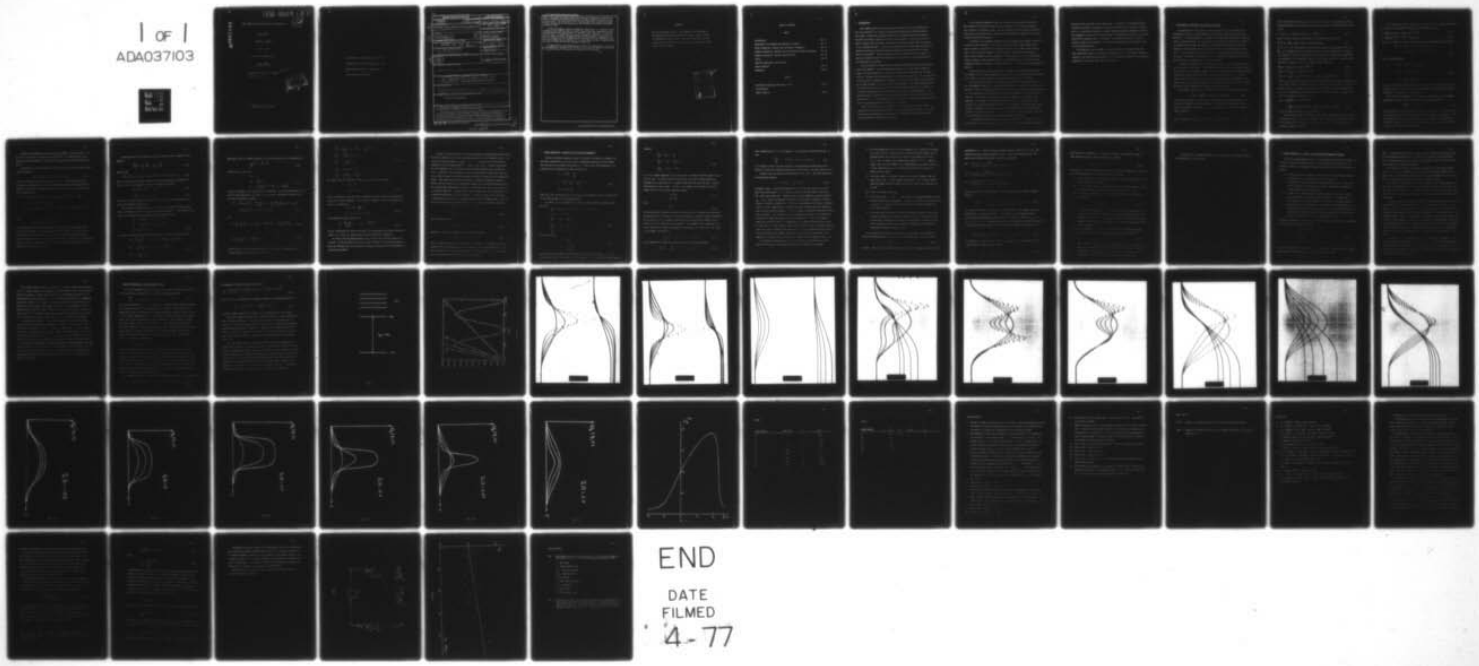

END

DATE FILMED
4-77

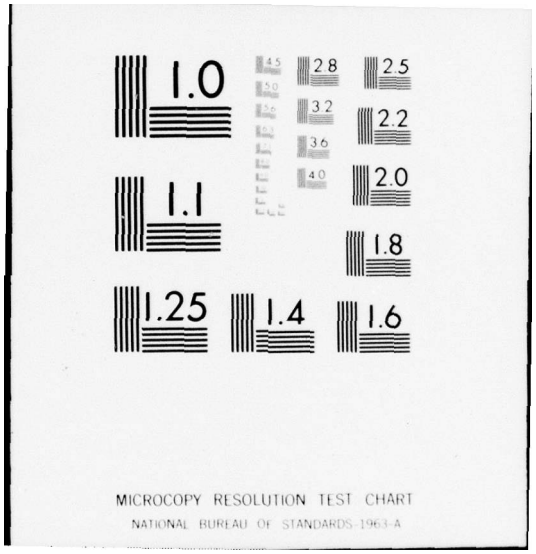
1.0
1.1
1.25
1.4
1.6
1.8
2.0
2.2
2.5
2.8
3.2
3.6
4.0
4.5
5.0
5.6
MICROCOPY RESOLUTION TEST CHART
NATIONAL BUREAU OF STANDARDS-1963-A

NON LINEAR OPTICAL AMPLIFICATION AND ABSORPTION

FINAL REPORT

LORENZO M. NARDUCCI

FEB. 25, 1977

U.S. ARMY RESEARCH OFFICE

GRANT NUMBER
DAA G29-76-G-0075

WORCESTER POLYTECHNIC INSTITUTE
Dept. of Physics

The findings in this report are not to be construed as an official department of the Army position, unless so designated by other authorized documents.

SECURITY CLASSIFICATION OF THIS PAGE (When Data Entered)

REPORT DOCUMENTATION PAGE

READ INSTRUCTIONS BEFORE COMPLETING FORM

1. REPORT NUMBER: P-13603-R-P
2. GOVT ACCESSION NO.: Final rept. 1 Jan - 31 Dec 76
3. RECIPIENT'S CATALOG NUMBER:

4. TITLE (and Subtitle): NON-LINEAR OPTICAL AMPLIFICATION AND ABSORPTION.
5. TYPE OF REPORT & PERIOD COVERED: Final Report Jan. 1-1976, Dec. 31-1976
6. PERFORMING ORG. REPORT NUMBER:

7. AUTHOR(s): Lorenzo M. Narducci
8. CONTRACT OR GRANT NUMBER(s): DAAG29-76-G-0075

9. PERFORMING ORGANIZATION NAME AND ADDRESS: Physics Department, Worcester Polytechnic Institute, Worcester, Mass. 01609 410101
10. PROGRAM ELEMENT, PROJECT, TASK AREA & WORK UNIT NUMBERS:

11. CONTROLLING OFFICE NAME AND ADDRESS: U. S. Army Research Office, Post Office Box 12211, Research Triangle Park, NC 27709
12. REPORT DATE: Feb. 25, 1977
13. NUMBER OF PAGES: 60p.

14. MONITORING AGENCY NAME & ADDRESS (if different from Controlling Office):
15. SECURITY CLASS. (of this report): Unclassified
15a. DECLASSIFICATION/DOWNGRADING SCHEDULE: NA

16. DISTRIBUTION STATEMENT (of this Report)

Approved for public release; distribution unlimited.

17. DISTRIBUTION STATEMENT (of the abstract entered in Block 20, if different from Report)

NA

18. ARO
19. 13603.1-R-P

18. SUPPLEMENTARY NOTES

The findings in this report are not to be construed as an official Department of the Army position, unless so designated by other authorized documents.

19. KEY WORDS (Continue on reverse side if necessary and identify by block number)

Two-Photon Amplification

20. ABSTRACT (Continue on reverse side if necessary and identify by block number)

This report summarizes the main results of ~~our~~ theoretical and experimental investigations on two-photon interaction processes.

~~Our~~ theoretical investigations have been directed to the analysis of the evolution of an optical pulse through a pumped medium which operates as a two-photon amplifier. The physical model under consideration consists of a collection of atoms prepared in a state of inversion between two levels of the same parity. An incident pulse with a carrier frequency approximately

next page

DD FORM 1 JAN 73 1473 EDITION OF 1 NOV 65 IS OBSOLETE

Unclassified

SECURITY CLASSIFICATION OF THIS PAGE (When Data Entered)

410101 1B

cont

equal to one-half the atomic transition frequency stimulates an induced non-linear polarization which oscillates with the same carrier frequency as the incident pulse. The evolution of the coupled atom-field system is described without restriction on the duration of the incident pulse and of the atomic relaxation times.

~~We show that~~ under coherent propagation conditions, i.e. when the pulse duration is much shorter than the atomic relaxation time, considerable pulse sharpening and power amplification is possible above threshold. In the rate equation limit, a regime where the atomic relaxation times are much shorter than the pulse duration, ~~we find that~~ optimum amplification conditions occur when the frequency of the incident pulse is detuned from its resonance value. The entire range from the coherent to the rate equation limit is explored with the help of hybrid and digital computer simulations.

~~Our~~ experimental investigations have lead to the measurement of the two-photon absorption constant in ZnS using a Q-switched ruby laser as the source. The measured value of the absorption constant is 0.013 cm/MW.

FOREWORDS

Due to the different nature of the theoretical and experimental investigations discussed in this report, we have decided to divide the presentation into two parts. Each part of the report is self-contained with its main text, figures and figure captions, as shown in the table of contents.

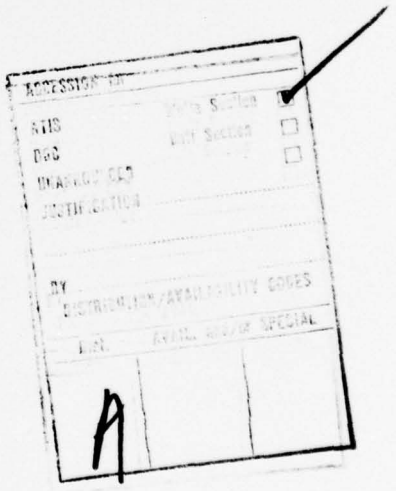

TABLE OF CONTENTS

PART I

PART II

1. Introduction

Laser amplification by two-photon stimulated decay was first considered in the early sixties[1,2] as a means of producing high peak-power radiation pulses. Since then, considerable progress has been made in understanding the dynamics of two-photon processes, especially in the coherent regime[3]. (The term coherent is used to signify that the atomic relaxation times are much longer than the duration of the propagating pulse.) Recent investigations have revealed numerous qualitative similarities between coherent two-photon absorption processes and their single-photon counterparts[4]. Little attention, however, has been paid to the physics of two-photon amplification,[5,6] and especially to the effects of atomic relaxation on the dynamics of the process.

Here we discuss the feasibility of producing laser amplification by two-photon stimulated emission. The active medium is modeled as a collection of identical atoms, initially prepared in a state of inversion between homogeneously broadened levels of the same parity, separated by a frequency difference ω_{ba}. We are especially concerned with the possibility of inducing a non-linear polarization which oscillates at the same frequency, $\omega \approx \frac{1}{2}\omega_{ba}$, as the incident pulse. The induced polarization is regarded as the source of a local field which adds coherently to the input wave to produce additional atomic polarization deeper in the amplifying medium. Our proposed scheme is based on the well known single-photon amplifier theory of Arecchi and Bonifacio[7]. In fact, similarities and differences between their results and ours will be repeatedly pointed out during our discussion.

There are, however, differences that are worth summarizing at the outset. For convenience we may distinguish between two different dynamical regimes. The first, called coherent propagation, occurs when the incident pulse is much shorter than the characteristic atomic relaxation times.

In the coherent propagation limit we find that an area equation, similar in some respects to the Arecchi-Bonifacio area equation, can be derived to predict the evolution of the pulse energy. Our area equation allows different steady state solutions for the pulse energy, unlike the Arecchi-Bonifacio equation which allows a unique steady state solution.

In addition, the threshold condition for power amplification imposes constraints on both the gain constant of the active medium and on the incident pulse energy. More precisely, we find that the two-photon amplifier has no small signal gain so that, even if the gain constant is large enough to allow power amplification, a weak incident pulse will not be amplified. On the contrary, if the incident pulse energy exceeds a certain threshold value, power amplification will occur with the subsequent formation of single or multiple-pulses in an analytically predictable fashion.

Unlike the case of the Arecchi-Bonifacio amplifier, no envelope steady state is possible for a two-photon amplifier because there is no power saturation mechanism in the model to limit the growth of the propagating pulse above threshold.

The rate equation regime offers additional interesting variations relative to the corresponding behavior of a single-photon amplifier. In the case of the Arecchi-Bonifacio theory, it is known that peak amplification occurs when the carrier frequency of the incident pulse coincides with the transition frequency of the two levels of interest. In our case we find that the frequency response of the system is not symmetric with respect to the detuning parameter $2\omega - \omega_{ba}$. In fact, for fixed values of the parameters characterizing the active medium, we find that power amplification is enhanced for positive values of the detuning parameter and depressed, instead, for negative values of $2\omega - \omega_{ba}$. This will be easily explained on the basis of the non-linear interaction mechanism proposed for the system.

Our discussion develops along the following main lines. In Section 2 we describe the basic features of the model, and derive the coupled propagation equations

that govern the evolution of the light pulse. In Section 3 we discuss the atomic relaxation mechanism, and compare the limiting coherent and rate equation regimes. Section 4 contains the results of a hybrid computer simulation designed to describe the propagation process for arbitrary values of the pulse duration and of the transverse atomic relaxation time. In Section 5 we discuss the details of the rate equation regime and the behavior of the amplification process for different values of the detuning parameter.

As indicated in the forewords, the last section of this report deals with some experimental aspects of two-photon absorption in ZnS. This subject being unrelated to the theoretical description of the two-photon amplifier will be discussed separately at the end of this report in Section 6.

2. Description of the Model and Equations of Motion.

Our formulation of the problem closely parallels the self-consistent field approximation theory of a single-photon laser amplifier advanced by Arecchi and Bonifacio[7]. In the same spirit, we visualize the amplification process as resulting from the following steps: an incident quasi-monochromatic light pulse of frequency ω impinges on the medium, it stimulates a macroscopic polarization at the same frequency, and interferes with the re-radiated field from the macroscopic polarization. The new total field repeats the cycle as it propagates through the medium. The system will behave as an amplifier, or as an absorber, depending on the relative phase between the incident and the re-radiated light.

Our system is assumed to be initially prepared in a state of inversion between two levels of the same parity. From a practical point of view, in order to maintain the inversion for a reasonable length of time, it is important that no dipole-allowed intermediate levels exist between the levels of interest (Fig. 1). It will be assumed here that the laser levels are the ground and first excited states of the active atoms. The levels are separated by an energy difference ω_{ba} and are coupled by dipole-allowed transitions to higher lying energy levels.

The incident electric field is assumed to be a quasi-monochromatic plane wave

$$\vec{\mathcal{E}}(x, t) = \vec{\mathcal{E}}_o(x, t)\cos(\omega t - kx + \varphi(x, t)) , \qquad (2.1)$$

where $\vec{\mathcal{E}}_o(x, t)$ and $\varphi(x, t)$ are slowly varying functions of space and time, ω is the carrier frequency, and k the propagation vector directed along the x axis. We choose a frequency ω such that $2\omega \approx \omega_{ba}$. The condition $2\omega = \omega_{ba}$ will be called two-photon resonance.

Let

$$|\psi(t)\rangle = \sum_j C_j(t)e^{-i\omega_j t}|j\rangle + C_a(t)e^{-i\omega_a t}|a\rangle + C_b(t)e^{-i\omega_b t}|b\rangle \qquad (2.2)$$

be the arbitrary state vector of an active atom, with $C_j(t)$, $C_a(t)$ and $C_b(t)$ slowly varying amplitudes. The evolution of the state vector (2.2) is induced by the Hamiltonian

$$H = E_a|a\rangle\langle a| + E_b|b\rangle\langle b| + \sum_j E_j|j\rangle\langle j| - \vec{p}\cdot\vec{\mathcal{E}}(x, t) \quad , \tag{2.3}$$

where the atomic polarization operator $\vec{p}$ is assumed to take the form

$$\vec{p} = \sum_j |a\rangle\langle j|\vec{p}_{aj} + \sum_j |b\rangle\langle j|\vec{p}_{bj} + \text{hermitian adjoint} \quad . \tag{2.4}$$

In eq. (2.4), we have neglected terms involving dipole matrix elements of the type $\vec{p}_{jj'}$ on the ground that the intermediate levels are never populated for a significant length of time, and interference effects between intermediate state amplitudes are negligible. The Schrodinger equation for the state vector (2.2) with the Hamiltonian (2.3) reduces to the set of coupled linear equations

$$i\hbar\dot{C}_a(t) = -\sum_j \mu_{aj}\mathcal{E}(x, t)C_j(t)e^{-i(\omega_j-\omega_a)t} \quad , \tag{2.5a}$$

$$i\hbar\dot{C}_b(t) = -\sum_j \mu_{bj}\mathcal{E}(x, t)C_j(t)e^{-i(\omega_j-\omega_b)t} \quad , \tag{2.5b}$$

$$i\hbar\dot{C}_j(t) = -\mu_{ja}\mathcal{E}(x, t)C_a(t)e^{-i(\omega_j-\omega_a)t} - \mu_{jb}\mathcal{E}(x, t)C_b(t)e^{i(\omega_j-\omega_b)t} \quad , \tag{2.5c}$$

where μ_{aj}, μ_{bj} are the projections of $\vec{p}_{aj}$ and $\vec{p}_{bj}$ along the direction of polarization of the field. Since we intend to focus our attention on the evolution of the amplitudes C_a and C_b, we eliminate the intermediate amplitudes by formally integrating eq. (2.5c) and substituting the result into eqs. (2.5a) and (2.5b). The new exact form of the equation of motion for C_a is

$$\dot{C}_a(t) = -\sum_j \frac{\mu_{aj}}{\hbar}\mathcal{E}(x, t)\, e^{-i\omega_{ja}t}\int_0^t dt'$$

$$\left(\frac{\mu_{ja}}{\hbar}\mathcal{E}(x, t')C_a(t')e^{i\omega_{ja}t'} + \frac{\mu_{jb}}{\hbar}\mathcal{E}(x, t')C_b(t')e^{i\omega_{jb}t'}\right) \quad . \tag{2.6}$$

A similar equation holds for the amplitude C_b.

At this point we make the slowly varying envelope approximation. This amounts to replacing $\mathcal{E}_o(x, t')$, $C_a(t')$, and $C_b(t')$ inside the integrals with their values at the upper limit of integration, and carrying out the exact integration of the remaining exponential factors.

After retaining the slowly varying terms, we arrive at the following equations of motion for the ground and excited state amplitudes C_a and C_b

$$\dot{C}_a = \frac{i}{\hbar}(k_{aa}|E_o|^2 C_a(t) + k_{ab}E_o^2 C_b e^{i(2\omega-\omega_{ba})t}) \quad , \tag{2.7}$$

$$\dot{C}_b = \frac{i}{\hbar}(k_{ab}E_o^{*2} C_a e^{-i(2\omega-\omega_{ba})t} + k_{bb}|E_o|^2 C_b) \quad . \tag{2.8}$$

In eq. (2.7) and (2.8) we have introduced the new field amplitude E_o defined by

$$\begin{aligned} \mathcal{E}(x,t) &= \mathcal{E}_o(x,t)\cos(\omega t - kx + \varphi) \\ &\equiv E_o(x,t)\, e^{i\omega t} + E_o^*(x,t)\, e^{-i\omega t} \quad , \end{aligned} \tag{2.9}$$

and the atomic parameters

$$\begin{aligned} k_{aa} &= \frac{2}{\hbar}\sum_j \mu_{ja}^2 \frac{\omega_{ja}}{\omega_{ja}^2 - \omega^2} \quad , \\ k_{bb} &= \frac{2}{\hbar}\sum_j \mu_{jb}^2 \frac{\omega_{jb}}{\omega_{jb}^2 - \omega^2} \quad , \\ k_{ab} &= \frac{1}{\hbar}\sum_j \frac{\mu_{ja}\,\mu_{jb}}{\omega_{ja} + \omega} \quad . \end{aligned} \tag{2.10}$$

It is worth pointing out that in the identification of the slowly varying terms leading to eqs. (2.7) and (2.8) we have excluded the possibility of accidental resonances of the type $|\omega_{ja}| \simeq \omega$, and $|\omega_{jb}| \simeq \omega$.

As a check of consistency on the adiabatic elimination of the intermediate amplitudes, we observe that the probability conservation statement

$$\frac{d}{dt}\left(|C_a|^2 + |C_b|^2\right) = 0 \tag{2.11}$$

follows directly from the equations of motion (2.7) and (2.8). At this point we are dealing, in effect, with a fictitious two-level system. The presence of the intermediate states is reflected indirectly in the quadratic field dependence exhibited in eqs. (2.7) and (2.8), a feature which is in sharp contrast with the results of the one-photon amplifier theory.

Guided by past experience with one-photon processes, one can cast eqs. (2.7) and (2.8) in the form of a Bloch set of equations[8]. The identification of the appropriate Bloch variables is aided by the calculation of the total polarization source.

By definition, if N is the number of atoms per unit volume, the atomic polarization is given by

$$P = N \langle p \rangle = N' \langle \psi(t) | p | \psi(t) \rangle \quad , \tag{2.12}$$

where $|\psi(t)\rangle$ is the state vector given by eq. (2.2). Upon elimination of the intermediate amplitudes $C_j(t)$, and after performing the slowly varying amplitude approximation as done in the derivation of eq. (2.7) and (2.8), the total polarization takes the form

$$\begin{aligned} P = {} & N \left\{ k_{aa} |C_a|^2 + k_{bb} |C_b|^2 + k_{ab} \left(C_a C_b^* e^{-i\alpha} + C_a^* C_b e^{i\alpha} \right) \right\} \\ & \times \mathcal{E}_0(x,t) \cos(\omega t - kx + \varphi) \\ & + N k_{ab} i \left(C_a C_b^* e^{-i\alpha} - C_a^* C_b e^{i\alpha} \right) \mathcal{E}_0(x,t) \sin(\omega t - kx + \varphi), \end{aligned} \tag{2.13}$$

where

$$\alpha = (2\omega - \omega_{ba})t - 2kx + 2\varphi \quad .$$

In close analogy with the one-photon amplifier theory, the atomic polarization contains one component which is in phase and one in quadrature with the driving electromagnetic field. In this case, however, the polarization components are explicitly proportional to the electric field envelope. Furthermore, the quadrature component, which is responsible for dispersion effects, depends also on the atomic population through $|C_a|^2$ and $|C_b|^2$.

The polarization (2.13) plays the role of the source term in Maxwell's wave equation

$$\frac{\partial^2 \mathcal{E}}{\partial x^2} - \frac{1}{c^2}\frac{\partial^2 \mathcal{E}}{\partial t^2} = \frac{1}{c^2 \epsilon_0}\frac{\partial^2 P}{\partial t^2} \quad . \tag{2.14}$$

Upon setting

$$P = P_s(x,t)\sin(\omega t - kx + \varphi) + P_c(x,t)\cos(\omega t - kx + \varphi) \quad , \tag{2.15}$$

where P_c and P_s are the slowly varying in phase and in quadrature components of P(x, t), eq. (2.14) reduces to the pair of transport equations

$$\mathcal{E}_0\left(c\frac{\partial \varphi}{\partial x} + \frac{\partial \varphi}{\partial t}\right) = -\frac{\omega}{2\epsilon_0} P_c \quad , \tag{2.16}$$

$$c\frac{\partial \mathcal{E}_0}{\partial x} + \frac{\partial \mathcal{E}_0}{\partial t} = -\frac{\omega}{2\epsilon_0} P_s \quad . \tag{2.17}$$

As usual, the field equations (2.16) and (2.17) are valid in the slowly varying amplitude and phase approximation.

The formal analogy between eqs. (2.7) and (2.8) and those describing single-photon transitions has been recognized by previous workers[3,4]. Such analogy is made especially transparent by introducing the new atomic variables

$$\begin{aligned} R_1 &= i\left(C_a^* C_b e^{i\alpha} - C_a C_b^* e^{-i\alpha}\right) \quad , \\ R_2 &= -\left(C_a C_b^* e^{-i\alpha} + C_a^* C_b e^{i\alpha}\right) \quad , \\ R_3 &= |C_b|^2 - |C_a|^2 \quad . \end{aligned} \tag{2.18}$$

In terms of these variables the atomic equations (2.7) and (2.8) take the form

$$\begin{aligned} \dot{R}_1 &= \left[\frac{k_{bb} - k_{aa}}{4\hbar}\mathcal{E}_0^2 + \left(2\omega - \omega_{ba} + 2\frac{\partial \varphi}{\partial t}\right)\right] R_2 + \frac{k_{ab}}{2\hbar}\mathcal{E}_0^2 R_3 \quad , \\ \dot{R}_2 &= -\left[\frac{k_{bb} - k_{aa}}{4\hbar}\mathcal{E}_0^2 + \left(2\omega - \omega_{ba} + 2\frac{\partial \varphi}{\partial t}\right)\right] R_1 \quad , \\ \dot{R}_3 &= -\frac{k_{ab}}{2\hbar}\mathcal{E}_0^2 R_1 \quad . \end{aligned} \tag{2.19}$$

Equations (2.19) are formally identical to the Euler equation for a precessing top

$$\frac{d}{dt}\vec{R} = \vec{\Lambda} \times \vec{R} \tag{2.20}$$

with $\vec{R} \equiv (R_1, R_2, R_3)$ and

$$\begin{aligned} \Lambda_1 &= 0 \quad , \\ \Lambda_2 &= \frac{k_{ab}}{2\hbar}\mathcal{E}_0^2 \quad , \\ \Lambda_3 &= -\left[\frac{k_{bb}-k_{aa}}{4\hbar}\mathcal{E}_0^2 + \left(2\omega - \omega_{ba} + 2\frac{\partial\varphi}{\partial t}\right)\right] . \end{aligned} \tag{2.21}$$

Clearly, the length of the Bloch vector is conserved. The atomic polarization (2.13) and the field equations (2.16) and (2.17) can also be expressed in terms of the new atomic variables as follows

$$\begin{aligned} \mathcal{P} = &-N k_{ab}\mathcal{E}_0\left[R_2 - \frac{k_{bb}-k_{aa}}{2k_{ab}}\left(R_3 + \frac{k_{aa}+k_{bb}}{k_{bb}-k_{aa}}\right)\right]\cos(\omega t - kx + \varphi) \\ &- N k_{ab}\mathcal{E}_0 R_1 \sin(\omega t - kx + \varphi) \quad , \end{aligned} \tag{2.22}$$

and

$$\left(c\frac{\partial}{\partial x} + \frac{\partial}{\partial t}\right)\left(2\omega - \omega_{ba} + 2\frac{\partial\varphi}{\partial t}\right) = \frac{\omega N k_{ab}}{\epsilon_0}\left(\dot{R}_2 - \frac{k_{bb}-k_{aa}}{2k_{ab}}\dot{R}_3\right) , \tag{2.23a}$$

$$\left(c\frac{\partial}{\partial x} + \frac{\partial}{\partial t}\right)\mathcal{E}_0^2 = \frac{\omega N k_{ab}}{\epsilon_0} R_1 \mathcal{E}_0^2 \quad . \tag{2.23b}$$

Finally, after a few minor changes of notation, we arrive at the entire set of coupled propagation equations for the amplifier

$$\frac{\partial R_1}{\partial \tau} = \left(\frac{\gamma}{\sqrt{1+\gamma^2}} \omega_R + \Omega \right) R_2 + \frac{\omega_R}{\sqrt{1+\gamma^2}} R_3 \quad ,$$

$$\frac{\partial R_2}{\partial \tau} = -\left(\frac{\gamma}{\sqrt{1+\gamma^2}} \omega_R + \Omega \right) R_1 \quad ,$$

$$\frac{\partial R_3}{\partial \tau} = -\frac{\omega_R}{\sqrt{1+\gamma^2}} R_1 \quad , \tag{2.24}$$

$$\frac{\partial \omega_R}{\partial \eta} = g \omega_R R_1 - \ell \omega_R \quad ,$$

$$\frac{\partial \Omega}{\partial \eta} = g \left(\frac{\partial R_2}{\partial \tau} - \gamma \frac{\partial R_1}{\partial \tau} \right) \quad .$$

The atomic and field variables evolve in the local reference system

$$\eta = \frac{x}{c}$$

$$\tau = t - \frac{x}{c} \quad , \tag{2.25}$$

which is traveling in the direction of propagation of the pulse with the speed of light in the inert background. The field Rabi frequency ω_R and the detuning parameter Ω are defined by

$$\omega_R = \sqrt{1+\gamma^2} \; \frac{k_{ab}}{2\hbar} \mathcal{E}_0^2 \quad ,$$

$$\Omega = (2\omega - \omega_{ba}) + 2 \frac{\partial \varphi}{\partial \tau} \quad . \tag{2.26}$$

The parameters γ and g are given by

$$\gamma = \frac{k_{bb} - k_{aa}}{2 k_{ab}} \quad , \quad g = \frac{\omega N' k_{ab}}{\epsilon_0} \quad . \tag{2.27}$$

Finally, ℓ describes all other non-resonant loss mechanisms (scattering, diffraction losses, etc.) which the incoming pulse suffers through the propagation.

We observe that ω_R depends quadratically on the field amplitude rather than linearly. We have decided to name ω_R the Rabi frequency of our problem because it plays an analogous role to the usual Rabi frequency introduced in the discussion of one-photon processes[8].

Certain differences between the two-photon amplifier equations and those derived by Arecchi and Bonifacio for the one-photon amplifier can be discussed at once. The effective detuning parameter $\frac{\gamma'}{\sqrt{1+\gamma^2}}\omega_R + \Delta$ is explicitly field-intensity dependent; the term proportional to ω_R plays the role of a dynamic Stark shift. The field equation for ω_R displays a field-intensity dependent gain coefficient. This indicates that the amplifier will not exhibit small signal gain, and that it will have an entirely different asymptotic (large η) behavior for the propagating pulse. Thus, while one of the main features of the Arecchi-Bonifacio amplifier theory was the prediction of a steady state pulse with an amplitude proportional to the instantaneous induced polarization, no such steady state pulse can be found for a two-photon amplifier. Finally, in the coherent regime (no atomic relaxation), the frequency detuning and the field intensity ω_R evolve, coupled to one another by a conservation law which is an exclusive feature of the two-photon model. This can be seen from the last two equations in (2.24). In fact the transport equations

$$\frac{\partial \omega_R}{\partial \eta} = -\gamma\, \omega_R\, R_3 - \ell\, \omega_R$$

$$\frac{\partial \Delta}{\partial \eta} = -\gamma\, \Delta\, R_3 \tag{2.28}$$

can be combined to give

$$\frac{\partial}{\partial \eta}(\omega_R \Delta) = -\ell\, \omega_R \Delta \quad . \tag{2.29}$$

Equation (2.29) can be integrated at once, with the result

$$(\omega_R \Delta)_\eta = (\omega_R \Delta)_{\eta=0}\, e^{-\ell\eta} \quad . \tag{2.30}$$

Hence, for sufficiently large distances into the amplifier, the detuning parameter vanishes, and the instantaneous carrier frequency of the field becomes $\frac{1}{2}\omega_{ba}$. On the other hand, if the incident signal satisfies the condition $\omega = \frac{1}{2}\omega_{ba}$, resonance will be maintained throughout the amplification process.

3. Atomic Relaxation. Coherent and Incoherent Propagation.

Before introducing relaxation terms for the atomic variables, we observe that the Bloch variables R_1, R_2 and R_3 are not fundamental parameters of the problem. The structure of the atomic polarization (2.22) and of the field equations (2.23) indicate that the appropriate atomic variables are

$$S = \sqrt{1+\gamma^2}\ \frac{R_1}{R_3^e} \quad ,$$

$$C = \sqrt{1+\gamma^2}\ \frac{R_2}{R_3^e} - \gamma\left(\frac{R_3}{R_3^e} - 1\right) \quad , \tag{3.1}$$

$$D = (1+\gamma^2)\ \frac{R_3}{R_3^e} - \gamma^2 \quad ,$$

where R_3^e is the equilibrium value of the population difference prior to the arrival of the leading edge of the propagating pulse.

In terms of the new variables the coupled Schrodinger-Maxwell equations take the form

$$\frac{\partial S}{\partial \tau} = (\Gamma\omega_R + \Omega)C + (\omega_R + \Gamma\Omega)D - \Gamma R - S/T_2 \quad ,$$

$$\frac{\partial C}{\partial \tau} = -\Omega S - C/T_2 \quad ,$$

$$\frac{\partial D}{\partial \tau} = -\omega_R S - \frac{1}{T_1}(D-1) \quad ,$$

$$\frac{\partial \omega_R}{\partial \eta} = G\omega_R S - \Gamma\omega_R \quad , \tag{3.2}$$

$$\frac{\partial \Omega}{\partial \eta} = -G\Omega S - \frac{G}{T_2}C \quad ,$$

where we have set

$$\Gamma = \frac{\gamma}{\sqrt{1+\gamma^2}} \quad ,$$

$$G = g\frac{R_3^e}{\sqrt{1+\gamma^2}} \quad , \tag{3.3}$$

and where we have introduced the phenomenological relaxation terms $\frac{S}{T_2}$, $\frac{C}{T_2}$, $\frac{D-1}{T_1}$ in the usual fashion. We observe that in resonance ($\Omega = 0$) the set of coupled equations

reduces to

$$\frac{\partial S}{\partial \tau} = \omega_R D - \frac{S}{T_2} \quad ,$$

$$\frac{\partial D}{\partial \tau} = -\omega_R S - \frac{1}{T_1}(D-1) \quad , \tag{3.4}$$

$$\frac{\partial \omega_R}{\partial \eta} = G \omega_R S - \ell \omega_R \quad ,$$

i.e. the in-phase component of the polarization C remains identically equal to zero for all time. In terms of these new variables, the formal analogy between the resonant set of equations for a two-photon amplifier and those derived by Arecchi and Bonifacio is even closer. In fact, if we neglect the relaxation terms, the formal solution of the atomic equations becomes

$$S = \sin \sigma \quad , \tag{3.5}$$

$$D = \cos \sigma \quad ,$$

where

$$\frac{\partial \sigma}{\partial \tau} = \omega_R \quad . \tag{3.6}$$

In the one-photon transition literature, σ (referred to as the pulse area) has played an important role in connection with the description of coherent transient phenomena. In the context of the two-photon transition theory an equivalent central role is played by the area under the pulse intensity. The resonant set of equations (3.4) can be reduced to a single area equation by using eqs. (3.5) and (3.6). The result of the simple calculation is

$$\frac{\partial^2}{\partial \tau \, \partial \eta} \sigma = G \sin \sigma \, \frac{\partial \sigma}{\partial \tau} - \ell \, \frac{\partial \sigma}{\partial \tau} \quad . \tag{3.7}$$

It is convenient to follow the evolution of the total integrated pulse

$$\sum (\eta) = \lim_{\tau \to \infty} \sigma(\eta, \tau) = \int_0^\infty \omega_R \, d\tau \quad . \tag{3.8}$$

Upon integrating eq. (3.7) with respect to τ and letting τ approach infinity, we find

$$\frac{\partial \Sigma}{\partial \eta} = -\ell \Sigma(\eta) + G(1 - \cos \Sigma(\eta)) \quad . \qquad (3.9)$$

It is simple to derive precise qualitative and quantitative predictions on the behavior of the total integrated pulse area on the basis of the area equation (3.9).

Consider first the steady state solutions of eq. (3.9). They must satisfy the transcendental equation

$$1 - \cos \Sigma(\eta) = \frac{\ell}{G} \Sigma(\eta) \quad . \qquad (3.10)$$

As shown in Fig. 2, non-trivial solutions to Eq. (3.10) will exist if the ratio $\frac{\ell}{G}$ is sufficiently small, i.e. if the gain parameter is sufficiently larger than the linear loss coefficient. Multiple roots are also apparent for small values of $\frac{\ell}{G}$. Fig. 2 shows the possible intersects of the straight line $\frac{\ell}{G}\Sigma$ for different values of the gain to loss ratio $\frac{G}{\ell}$. The three cases shown in the figure correspond to $\frac{G}{\ell}$ = 1, 2 and 5 respectively. A simple stability argument shows that beginning with the trivial stable solution $\Sigma = 0$, the stable and unstable solutions alternate with one another. The actual value of the asymptotic solution $\Sigma(\infty)$ is determined by the gain to loss ratio and by the initial value of Σ. Thus, for example, a pulse with an initial area $\Sigma(0) = 3$ propagating in a medium characterized by a gain to loss ratio of 5 will continue to grow until its area reaches the stable asymptotic value 4.76, while a pulse with an input area $\Sigma(0) = 6$ will experience power amplification (as shown by the computer solutions of the full set of equations) with a reduction of the pulse area from the initial value 6 to the asymptotic value 4.76.

The general conclusions that can be reached from the analysis of the area equation (3.9) and of its asymptotic solutions are summarized as follows:

i) Two requirements must be met for the propagation of a pulse with an asymptotic area $\sum(\infty) \neq 0$. First the gain to loss ratio must be larger than a threshold value (the inverse of the slope of the dashed line in Fig. 2, $\frac{G}{\ell} \geq 1.38$). Secondly, the incident pulse energy ($\sum(0)$) must be larger than the first unstable root corresponding to the given choice of $\frac{G}{\ell}$. If both conditions are met, the total pulse energy will converge to a stable non-zero value.

ii) The output value of the pulse energy can be larger or smaller than the input value $\sum(0)$. In both cases, the solution of the coherent resonant equations shows that power amplification will occur if the conditions (i) are met.

iii) There is no small signal gain.

iv) It is anticipated, and confirmed by the computer simulation, that multiple pulses can be propagated. In fact, we find that if a pulse evolves to an area $\sum$ given by the n-th stable root, the pulse will split into (n-1) distinct pulses.

v) It is also anticipated that no steady state pulse envelope will be found. This is confirmed by the computer simulation, where it is seen that when the threshold conditions are satisfied, the peak power continues to grow, while the pulse duration becomes smaller and smaller as the pulse area approaches its stable asymptotic value.

We consider now the extreme limiting case of very short atomic relaxation times (rate equation limit). From eq. (3.2) we can see that, if $\frac{\partial \sigma}{\partial \tau} \simeq 0$, then

$$\frac{\partial \Delta^2}{\partial \eta} = 0 \tag{3.11}$$

as well. Hence, in the incoherent propagation limit the detuning parameter becomes

independent of η. This is in sharp contrast with the result of eq. (2.30), which characterizes the coherent propagation limit. In the rate equation limit, the steady state values of the atomic variables are given by

$$S = \frac{T_2\,\omega_R}{1 + T_1 T_2\,\omega_R(\omega_R + \Gamma\Omega) + T_2^2\,\Omega(\Gamma\omega_R + \Omega)}\,,$$

$$C = -\frac{T_2^2\,\Omega\,\omega_R}{1 + T_1 T_2\,\omega_R(\omega_R + \Gamma\Omega) + T_2^2\,\Omega(\Gamma\omega_R + \Omega)}\,, \qquad (3.12)$$

$$D = \frac{1 + T_2^2\,\Omega(\Gamma\omega_R + \Omega) + \Gamma\,\Omega\,T_1 T_2\,\omega_R}{1 + (\Gamma\omega_R + \Omega)\,T_2^2\,\Omega + (\omega_R + \Gamma\Omega)\,T_1 T_2\,\omega_R}\,.$$

The evolution of the field variable ω_R is described by the non-linear transport equation

$$\frac{\partial\,\omega_R}{\partial\,\eta} = G\,\frac{T_2\,\omega_R^2}{1 + T_1 T_2\,\omega_R(\omega_R + \Gamma\Omega) + T_2^2\,\Omega(\Gamma\omega_R + \Omega)} - \ell\,\omega_R\,. \qquad (3.13)$$

It is easy to see that, even in the rate equation limit, small signal gain is not possible for a two-photon amplifier. Each segment of the propagating pulse can be viewed as propagating independently of the others according to eq. (3.13). If $\omega_R(\eta = 0, \tau) = \omega_R^0(\tau)$ represents the input field intensity at a particular position from the pulse leading edge, it is easy to see that amplification will occur if

$$\frac{G}{\ell}\,\frac{T_2\,\omega_R^0}{1 + T_1 T_2\,\omega_R^0(\omega_R^0 + \Gamma\Omega) + T_2^2\,\Omega(\Gamma\omega_R^0 + \Omega)} > 1\,. \qquad (3.14)$$

In resonance ($\Omega = 0$) it is clear that the condition $\frac{G}{\ell} > 1$ is not sufficient for amplification. Indeed, one must require

$$\frac{G}{\ell}\,\frac{T_2\,\omega_R^0}{1 + T_1 T_2\,(\omega_R^0)^2} > 1\,, \qquad (3.15)$$

which may not be satisfied for ω_R^0 sufficiently small. Surprisingly enough, a large signal is also not amplified unless the condition

$$\frac{G}{\ell} \frac{1}{T_1 \omega_R^0} > 1 \tag{3.16}$$

is satisfied. In the rate equation limit and for resonant propagation, our qualitative analysis points to the following general conclusions:

i) The leading edge of the propagating pulse is always absorbed by the action of the linear loss mechanism.

ii) If the gain to loss ratio is sufficiently large, amplification will occur for those values of the pulse intensity that satisfy eq. (3.15).

iii) As the pulse intensity $\omega_R(\eta,\tau)$ increases, a steady state condition is reached when

$$\frac{G}{\ell} \frac{T_2 \omega_R^{2s}}{1 + T_1 T_2 (\omega_R^{2s})^2} = 1 \quad . \tag{3.17}$$

Since the steady state value ω_R^{2s} is only a function of the gain to loss ratio and of the atomic relaxation times, it is predicted that pulse reshaping will take place with the pulse leading and trailing edges becoming sharper and the pulse-top flattening out. On the other hand, pulse splitting will be impossible.

iv) Out of resonance $(\Delta \neq 0)$ it is predicted that the maximum pulse growth rate will occur at the intensity dependent value of the detuning

$$\Delta_{max} = \pm \frac{1}{2} \left(\frac{T_2}{T_1} + 1 \right)^{1/2} \omega_R \quad . \tag{3.18}$$

Thus, unlike the case of the single-photon amplifier, the frequency dependence of the instantaneous gain is not symmetric about $\Delta = 0$. This lack of symmetry is also exhibited by the dispersion characteristics of the steady state values of the atomic variables given by eqs. (3.12).

The details of our computer simulation of the coherent and incoherent regimes are discussed in Sections 4 and 5.

4. Computer Simulation. Coherent and Intermediate Propagation Regimes.

The set of coupled equations (3.2) have been analyzed with a hybrid computer for a variety of choices of the parameters. We have limited our simulations to the resonant condition, and investigated the following main features of the propagation problem:

i) A verification of the analytic prediction that if the detuning parameter Ω is initially zero, it remains zero for every value of η.

ii) An analysis of the threshold conditions discussed in Section 3 and of the relation between the input pulse area and the propagation of single and multiple pulses in the coherent limit.

iii) A study of the transient pulse modulation occurring even when a single pulse is expected to propagate along the amplifier. In particular, we have focused on the atomic relaxation effects on the envelope modulation.

iv) Power amplification and approach to equilibrium of the pulse energy. As already pointed out, the pulse peak power will increase above threshold with an increase or decrease of the total energy depending on the gain to loss ratio of the amplifier and on the incident pulse energy.

The physical system is assumed to be excited in a swept excitation mode corresponding to the initial and boundary conditions

$$S(\eta, \tau=0) = C(\eta, \tau=0) = 0 \quad ,$$

$$D(\eta, \tau=0) = 1 \quad ,$$

$$\Omega(\eta=0, \tau) = 0 \quad , \qquad (4.1)$$

$$\omega_R(\eta=0, \tau) = \omega_{p0}\tau \quad .$$

The initial population is inverted, i.e. the parameter G is positive, and the input pulse envelope is assumed to have the convenient analytic form

$$\omega_p(\tau) = \omega_{p0} \sin^2\left(\pi \frac{\tau}{\tau_p}\right) \quad , \qquad (4.2)$$

where τ_p denotes the duration of the pulse from the leading to the trailing edge. The longitudinal relaxation time T_1 is taken to be infinite in this simulation, while T_2 has been varied over two orders of magnitude to explore the entire range from coherent to incoherent propagation.

As a result of the choice of boundary conditions for the detuning parameter ($\Omega(\eta = 0, \tau) = 0$) it is expected that both Ω and the in-phase component of the polarization should remain identically equal to zero throughout the entire propagation. This prediction has been verified to excellent accuracy.

The results of our analysis can be grouped into two main classes depending on the choice of the input area $\Sigma(0)$ and of the gain to loss ratio (a summary of the input data is given in Table I). For fixed values of $\Sigma(0)$ and G/ℓ we have varied the ratio T_2/τ_p to simulate the different effects of atomic relaxation on the pulse propagation.

In Figs. 3 through 5 we show the evolution of an incident pulse of area $\Sigma(0) = 3$ propagating in a medium characterized by a gain to loss ratio equal to 2. Upon inspection of Fig. 2 we see that for $G/\ell = 2$ and for an input area larger than the threshold value, a single peak is expected to propagate in the coherent limit. This is shown clearly in Fig. 3. By contrast, we see that for the same gain to loss ratio, but with a larger input area ($\Sigma(0) = 8$) considerable envelope modulation is present in the coherent limit (Fig. 6). Since, however, in the coherent limit the asymptotic value of the pulse area $\Sigma(\infty)$ is controlled only by the ratio G/ℓ, the asymptotic values of Σ for the cases displayed in Fig. 3 and 6 have been verified to be the same.

As the ratio T_2/τ_p is made smaller (Fig. 4) a considerable sharpening of the pulse is observed corresponding to a larger fraction of the incident pulse being below threshold for amplification. For even smaller values of T_2 there is not enough gain in the system to support amplification and the entire pulse is dissipated out by the linear loss mechanism (Fig. 5).

For a larger value of the gain to loss ratio, multiple steady state solutions for $\Sigma(\infty)$ become possible. The computer simulation indicates that in the coherent regime the existence of (n+1) stable roots of the transcendental equation (3.10) (including the trivial solution $\Sigma(\infty) = 0$) implies the possibility of propagating pulses which exhibit up to n peaks. The general rule that has emerged out of our analysis is that the pulse whose asymptotic area $\Sigma(\infty)$ corresponds to the n-th stable root will show (n-1) peaks. Thus, for a gain to loss ratio of 5 and for an input area $\Sigma(0) = 9.8$, stable double peak propagation is expected in the coherent limit. This is shown in Fig. 7 where the ratio T_2/τ_p is taken to be infinite.

For decreasing values of T_2 the envelope modulation becomes less and less pronounced until the second peak disappears altogether. This is shown in Figs. 8 and 9 where the values of T_2/τ_p are 1.25 and 0.13, respectively. Upon decreasing T_2 even further, the amplifier can no longer support power amplification and the entire pulse dies off as shown in Fig. 10 ($T_2/\tau_p = 0.038$). The rate equation (3.13) indicates that if the gain G is made sufficiently large to compensate for the decrease in the polarization relaxation time, power amplification becomes possible once again. This is confirmed in Fig. 11 where T_2/τ_p is kept equal to 0.038 (as in Fig. 10), but the gain to loss ratio is increased to 12. In this case the amplified pulse is more symmetric and it evolves in much the same way as in the rate equation limit discussed in Section 5.

5. Computer Simulation. The Rate Equation Limit.

In the rate equation limit the evolution of the atomic variables is controlled by the steady state solutions (3.12) and by the transport equation

$$\frac{\partial \omega_R}{\partial \eta} = \frac{G\, T_2\, \omega_R^2}{1 + T_1 T_2\, \omega_R (\omega_R + \Gamma_{12}) + T_2^2 \Omega^2 (\Gamma_{12}\omega_R + \Omega^2)} - \ell\, \omega_R \qquad (5.1)$$

for the field intensity $\omega_R(\eta, \xi)$. Equation (5.1) indicates that different portions of the pulse envelope evolve independently of one another. This eliminates the possibility of pulse envelope modulation and multiple peak formation which is typical of the coherent propagation regime. In addition, different sections of the input pulse with the same intensity will evolve identically. Thus, a symmetric pulse will evolve symmetrically for all values of η. It is simple to establish the threshold condition for amplification from Eq. (3.13). As expected, a sufficiently large value of the gain to loss ratio G/ℓ will not be enough for the pulse to undergo amplification; instead, one must require that the local instantaneous value of ω_R satisfy the inequality

$$\frac{G}{\ell} \frac{T_2\, \omega_R}{1 + T_1 T_2\, \omega_R (\omega_R + \Gamma_{12}) + T_2^2 \Omega^2 (\Gamma_{12}\omega_R + \Omega^2)} > 1 \,. \qquad (5.2)$$

Thus, the leading and trailing edges of the pulse are always absorbed. Unlike the case of the coherent propagation limit the pulse envelope does not sharpen up indefinitely, but rather it approaches a rectangular steady state shape, the pulse height being characterized by the asymptotic value of ω_R which satisfies the condition $\frac{\partial \omega_R}{\partial \eta} = 0$. This qualitative picture is only approximately true, and fails to account for the pulse evolution when the rise time of the leading edge and the decay time of the trailing edge become comparable to T_2.

The threshold intensity ω_R^{th} can be easily computed from Eq. (5.2). The result is

$$\omega_R^{th} = \frac{\left(\frac{G}{\ell} - \left(\frac{T_1}{T_2} + 1\right)\Gamma T_1 \Omega^2\right) - \left[\left(\frac{G}{\ell} - \left(\frac{T_1}{T_2} + 1\right)\Gamma T_1 \Omega^2\right)^2 - 4\frac{T_1}{T_2}\left(1 + T_2^2 \Omega^2\right)\right]^{1/2}}{2\, T_2} \qquad (5.3)$$

The asymptotic steady state value is given by

$$\omega_R^{ss} = \frac{\left(\frac{G}{\ell} - \left(\frac{T_1}{T_2}+1\right)\Gamma T_2 \Omega\right) + \left[\left(\frac{G}{\ell} - \left(\frac{T_1}{T_2}+1\right)\Gamma T_2 \Omega\right)^2 - 4\,\frac{T_1}{T_2}\left(1+T_2^2\Omega^2\right)\right]^{1/2}}{2\,T_1} \quad . \tag{5.4}$$

From Eq. (5.3) we conclude that a necessary condition for pulse amplification is

$$\frac{G}{\ell} > \left(\frac{T_1}{T_2}+1\right)\Gamma T_2 \Omega + 2\sqrt{\frac{T_1}{T_2}\left(1+T_2^2\Omega^2\right)} \quad . \tag{5.5}$$

A second necessary condition, of course, is the validity of Eq. (5.3) itself.

A detailed computer analysis of the transport equation (5.1) has confirmed the above threshold conditions. A few typical solutions are displayed in Fig. 12 through 17, with the input pulse plotted together with two amplified (or absorbed) pulses further down along the amplifier (a summary of the input data is given in Table 2). The gain to loss ratio, the ratio T_1/T_2 and the parameter Γ have been kept fixed, while the detuning Ω has been varied on either side of the resonant value $\Omega = 0$.

The most obvious feature of these solutions is the lack of symmetry in the amplification process for incident pulses that are removed from resonance by equal amounts in opposite directions. This is made explicit in Fig. 18 where the maximum pulse intensity from a fixed length of amplifying medium is plotted as a function of detuning. It is clear that the maximum amplification occurs for values of the detuning that are different from zero. In the present computer simulation, the parameter Γ is negative. If we had chosen a positive value for Γ, the maximum amplification would have occurred for negative values of the detuning Ω.

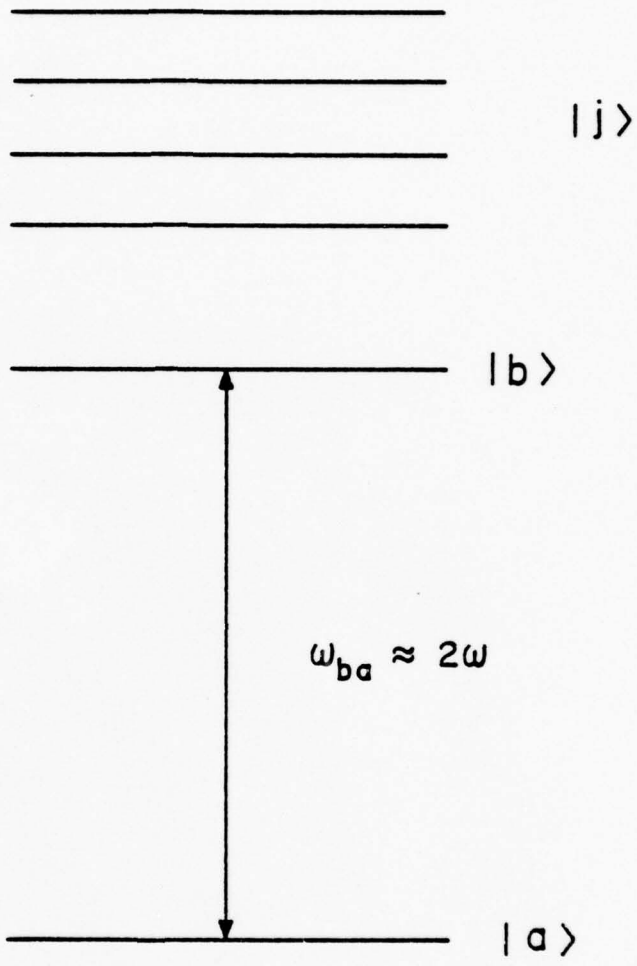

FIG. # 1

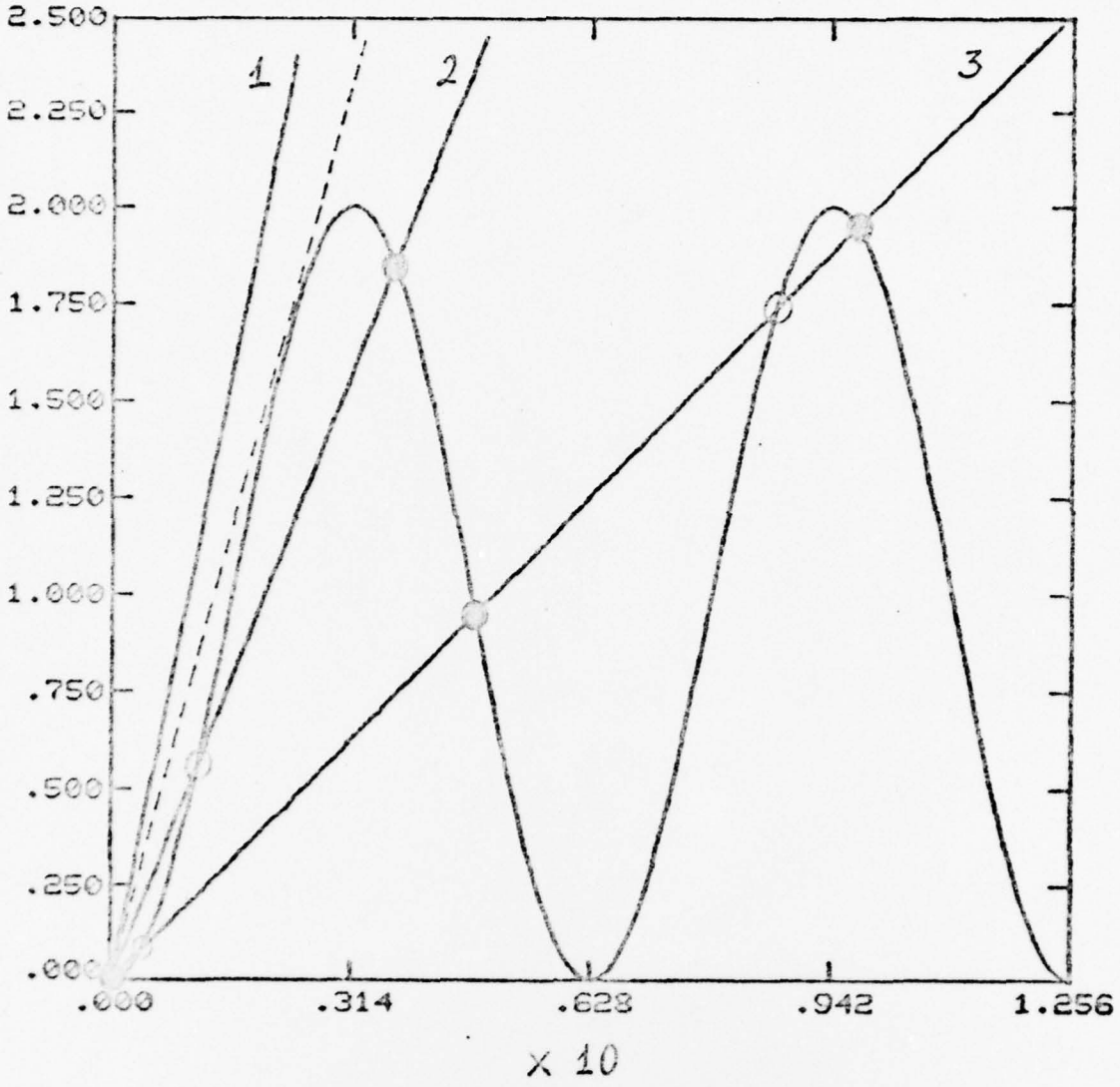
2.500
2.250
2.000
1.750
1.500
1.250
1.000
.750
.500
.250
.000
1
2
3
.000
.314
.628
.942
1.256
X 10

FIG. # 2

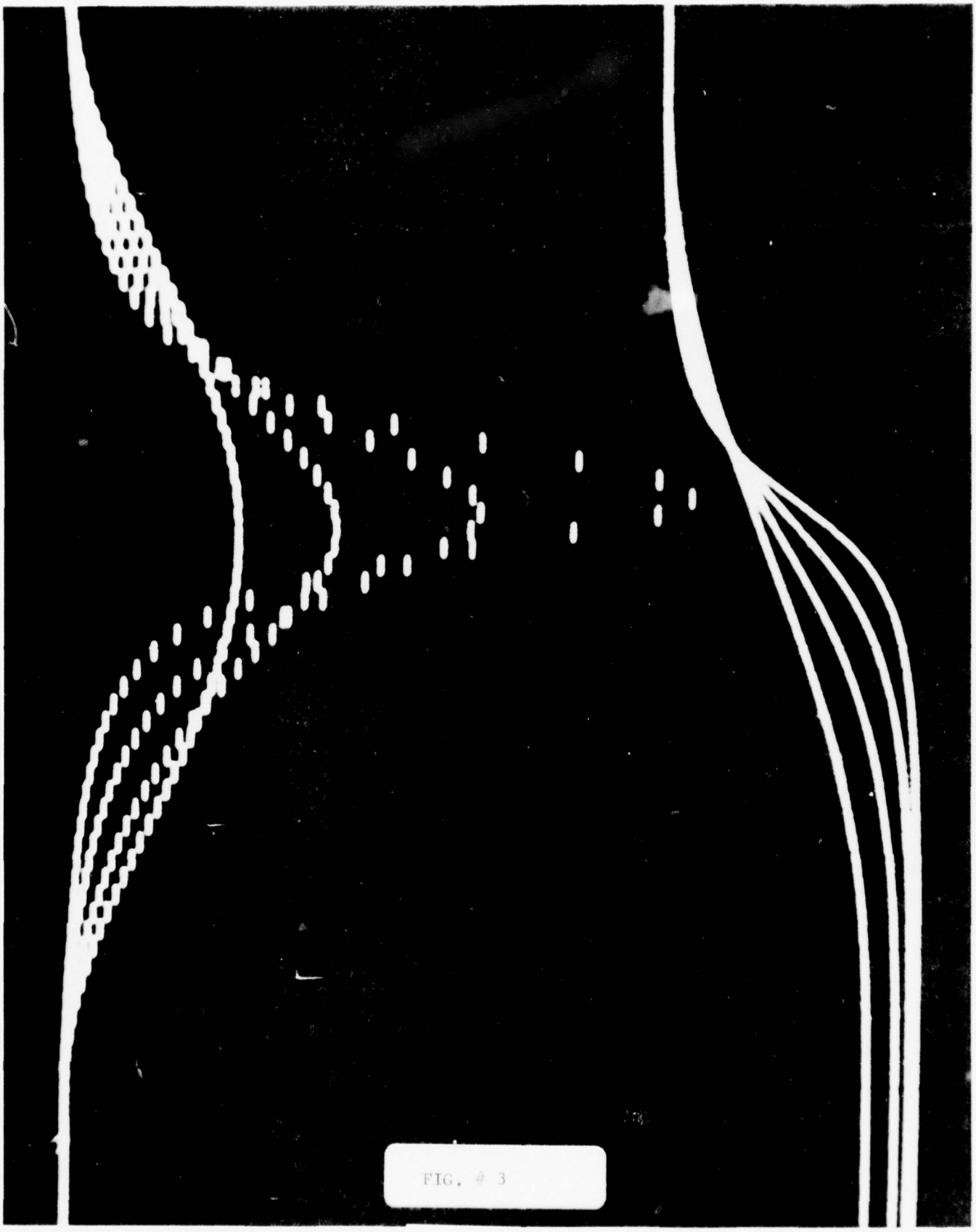

FIG. # 3

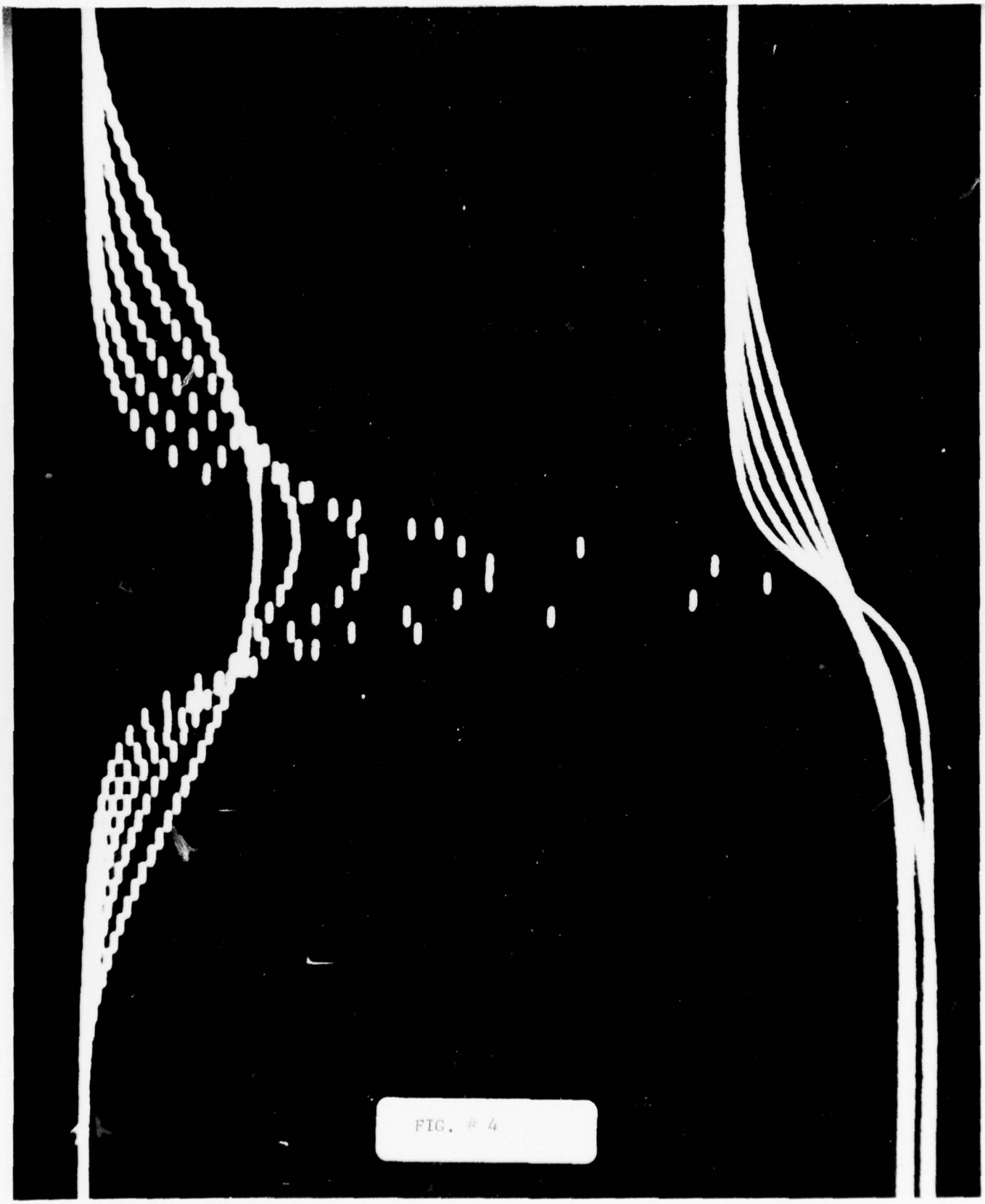

FIG. # 4

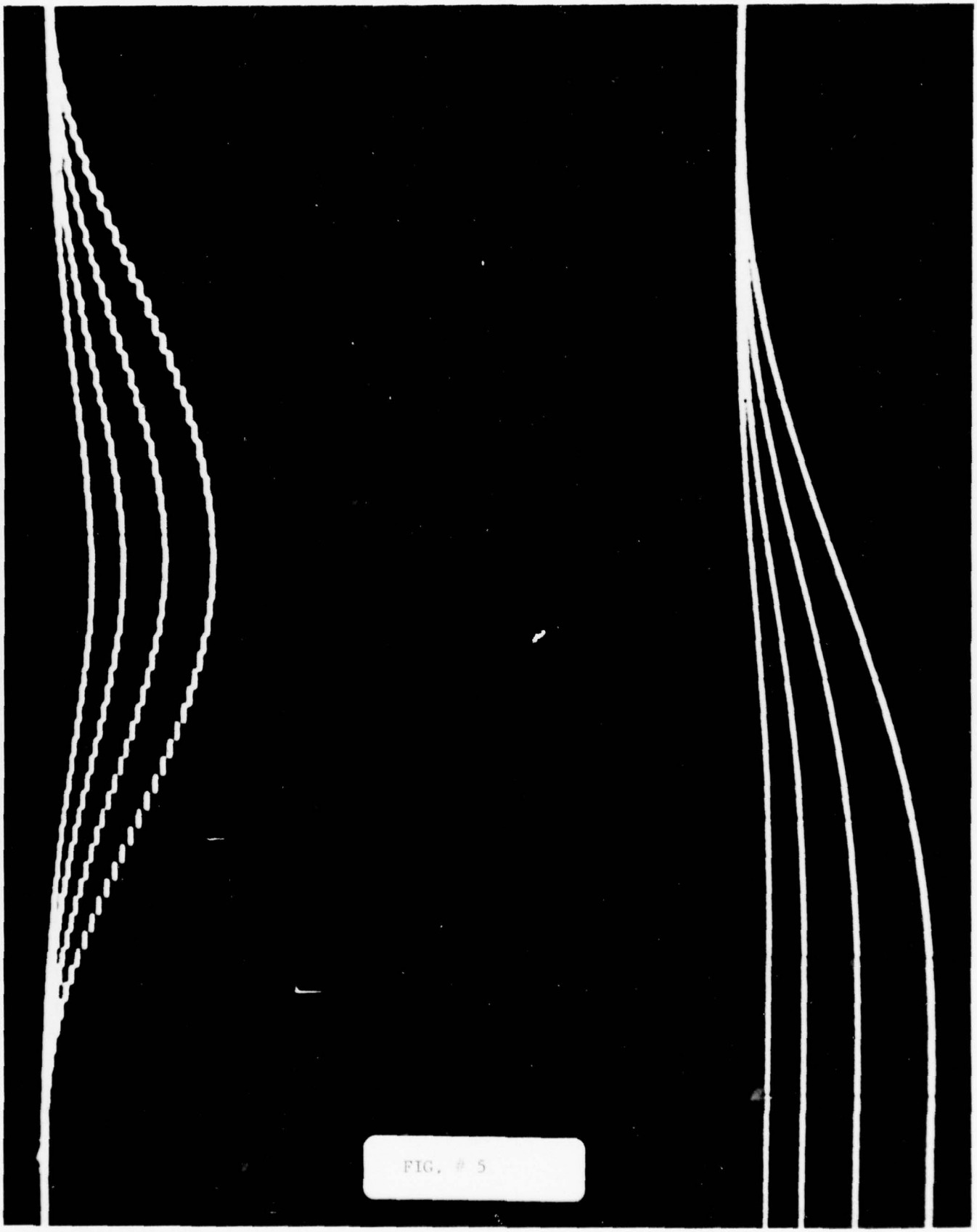

FIG. # 5

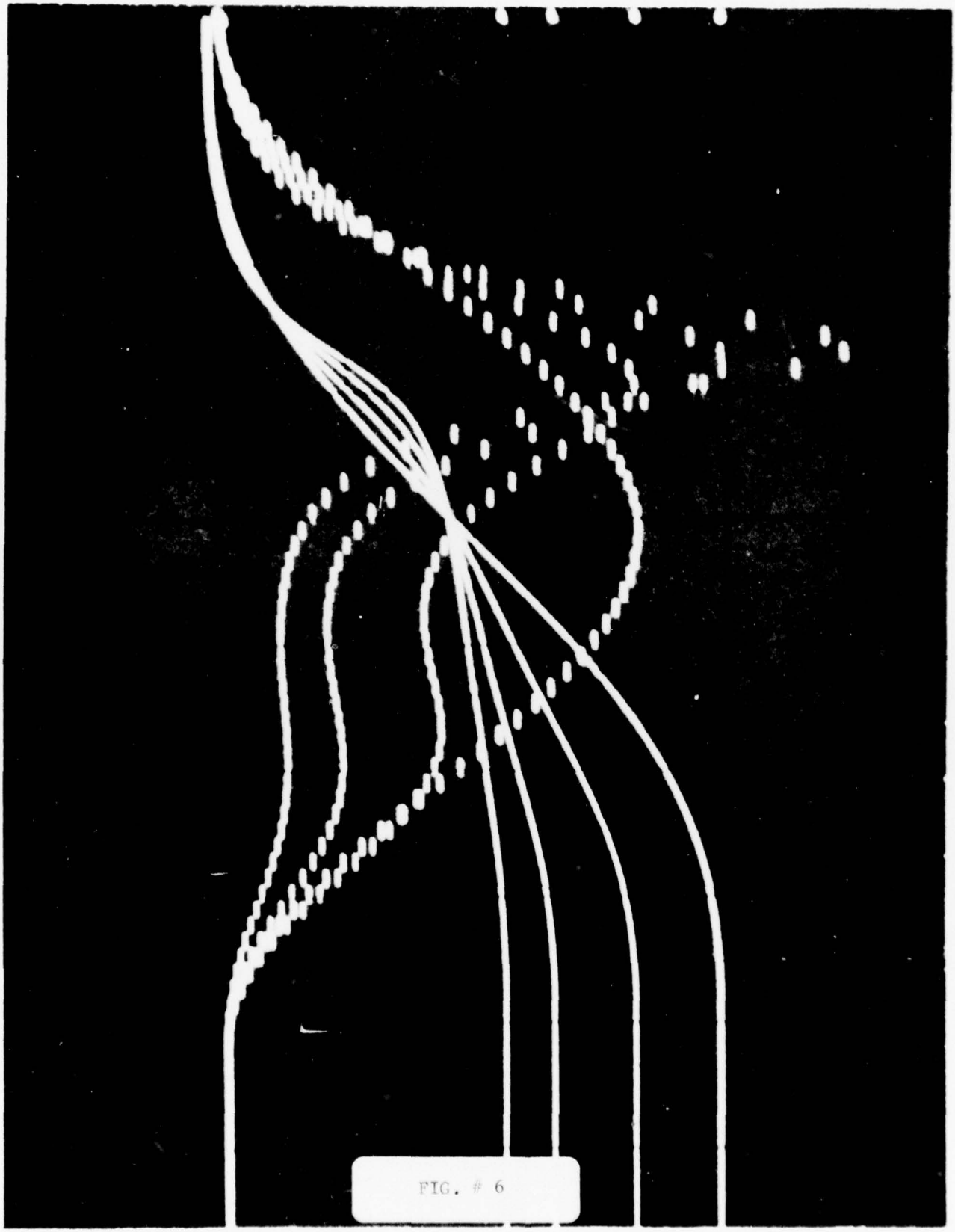

FIG. # 6

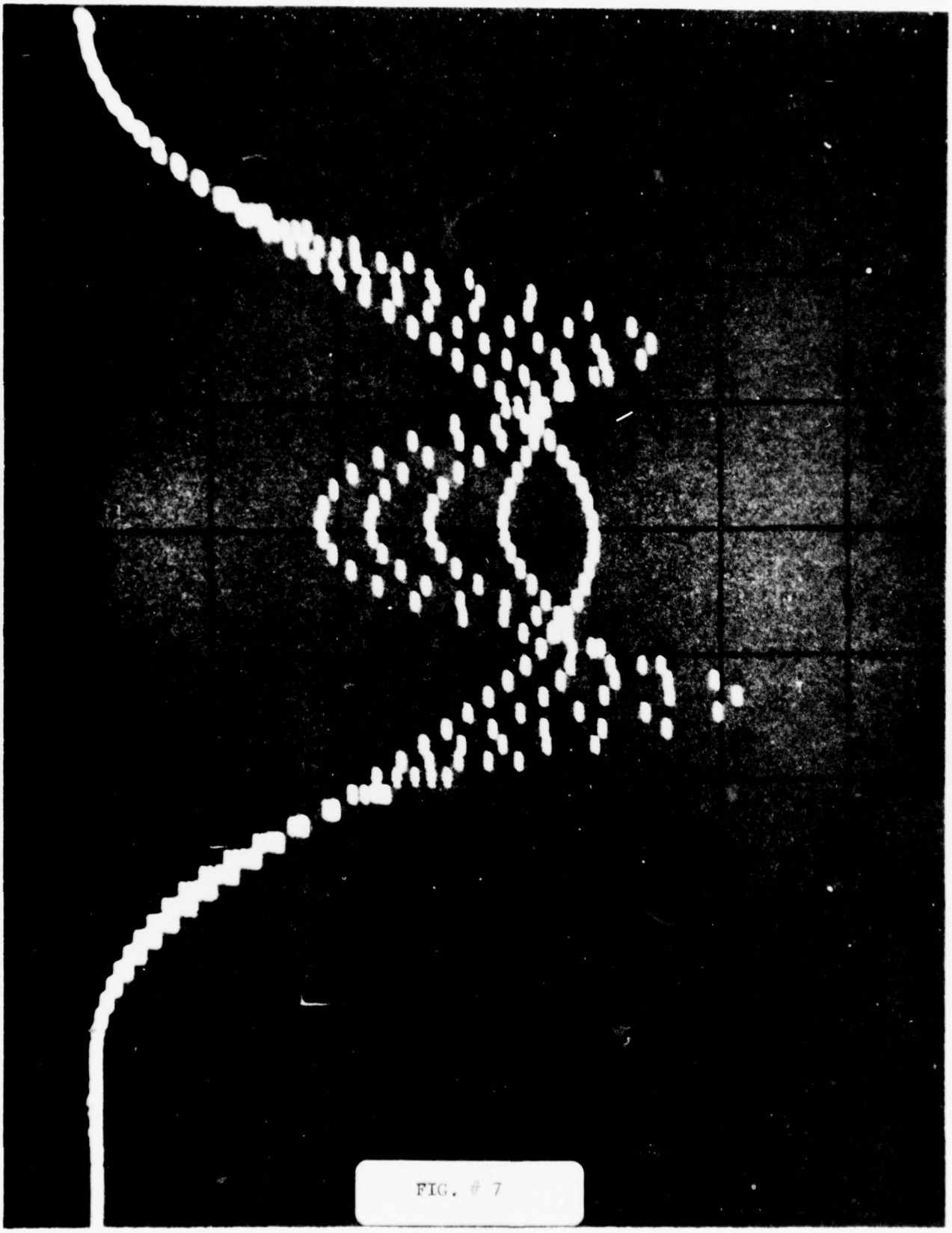

FIG. # 7

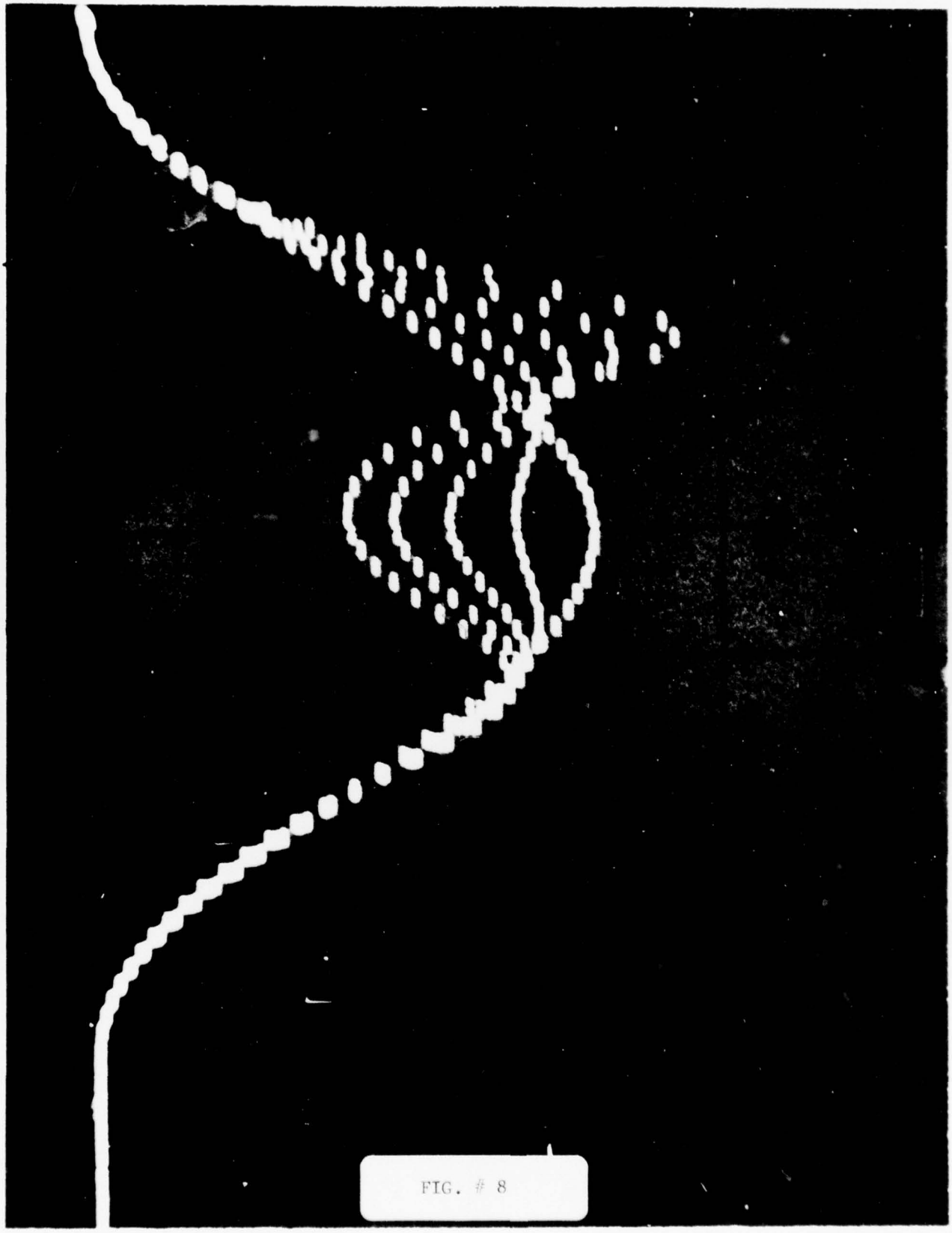

FIG. # 8

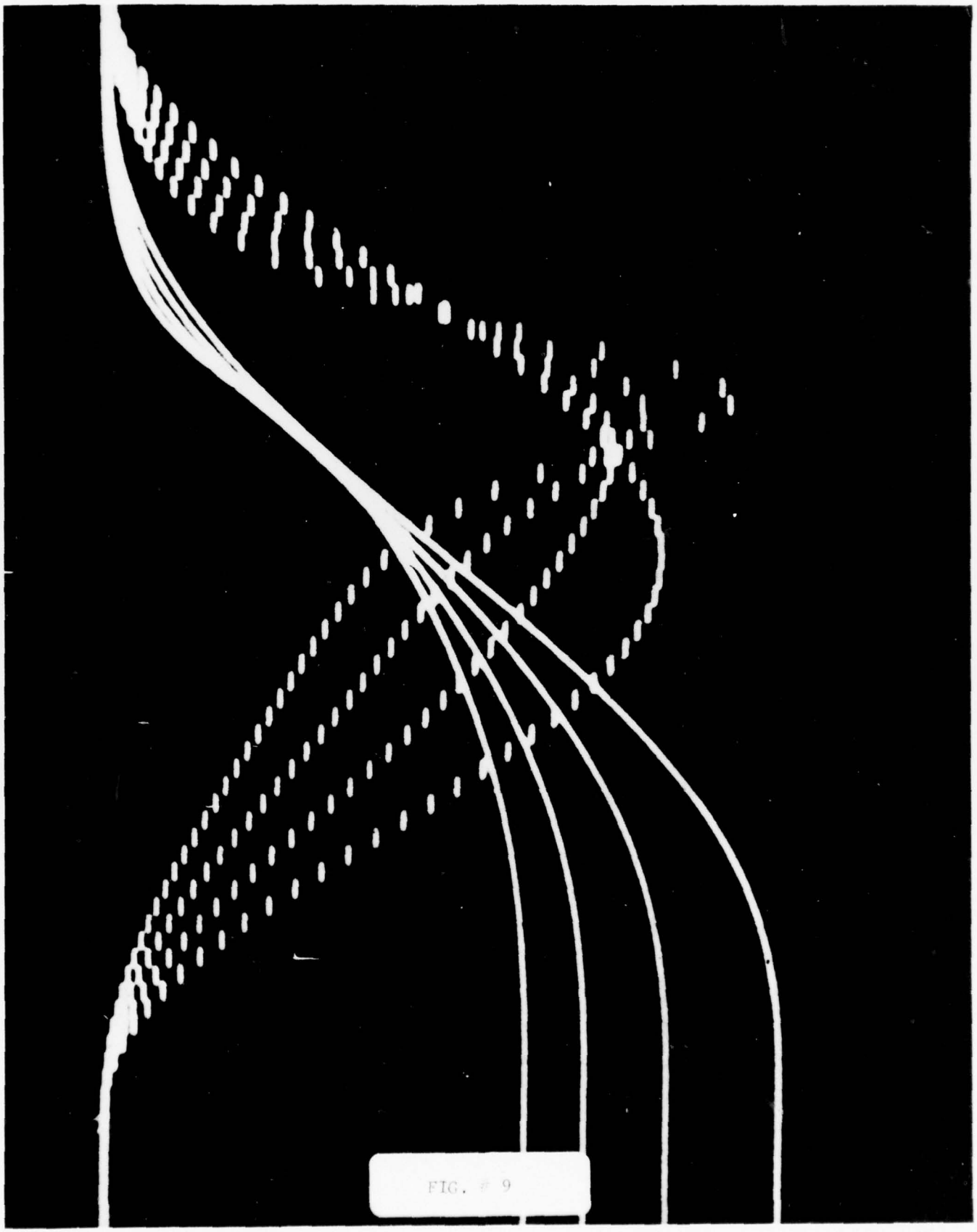

FIG. # 9

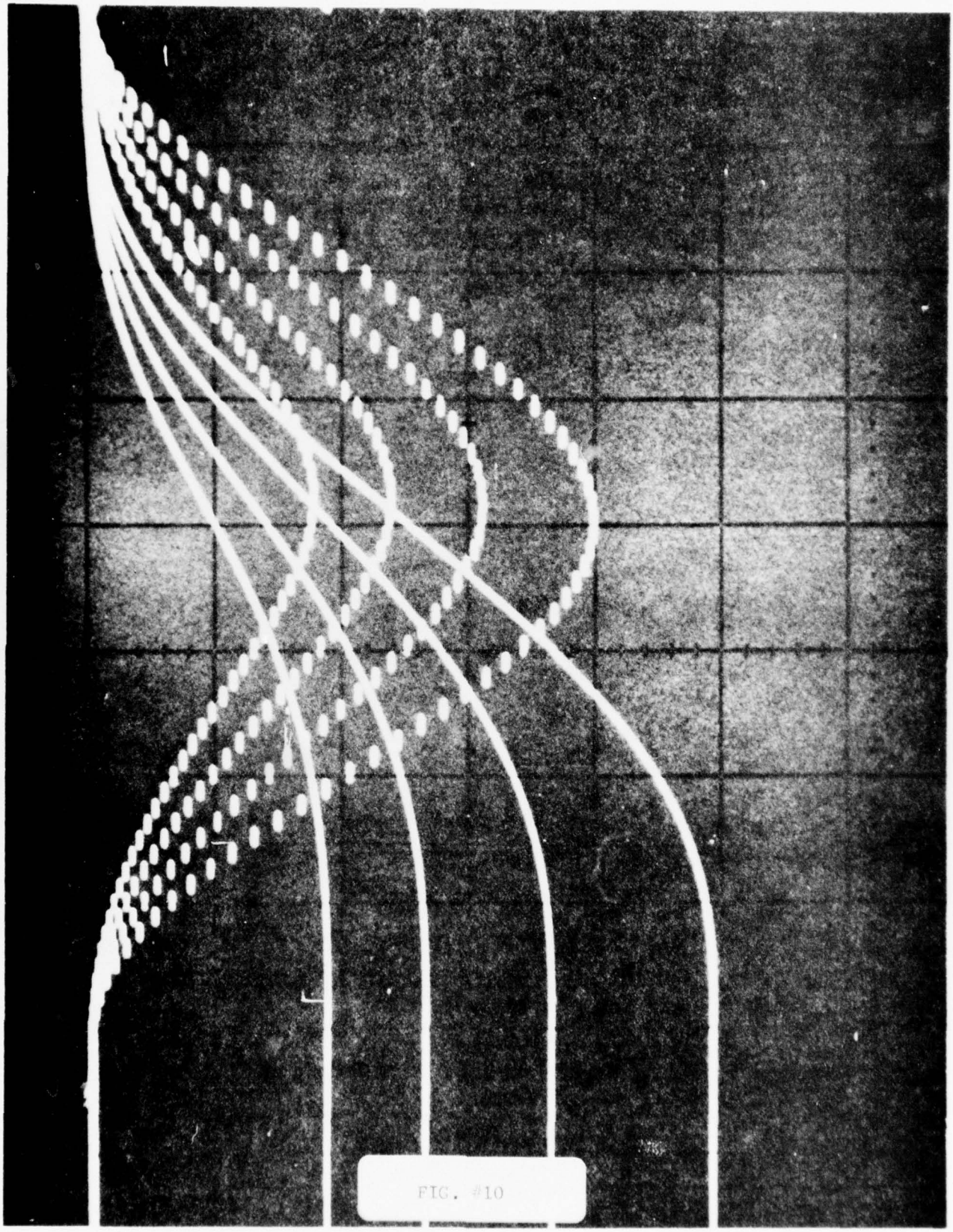

FIG. #10

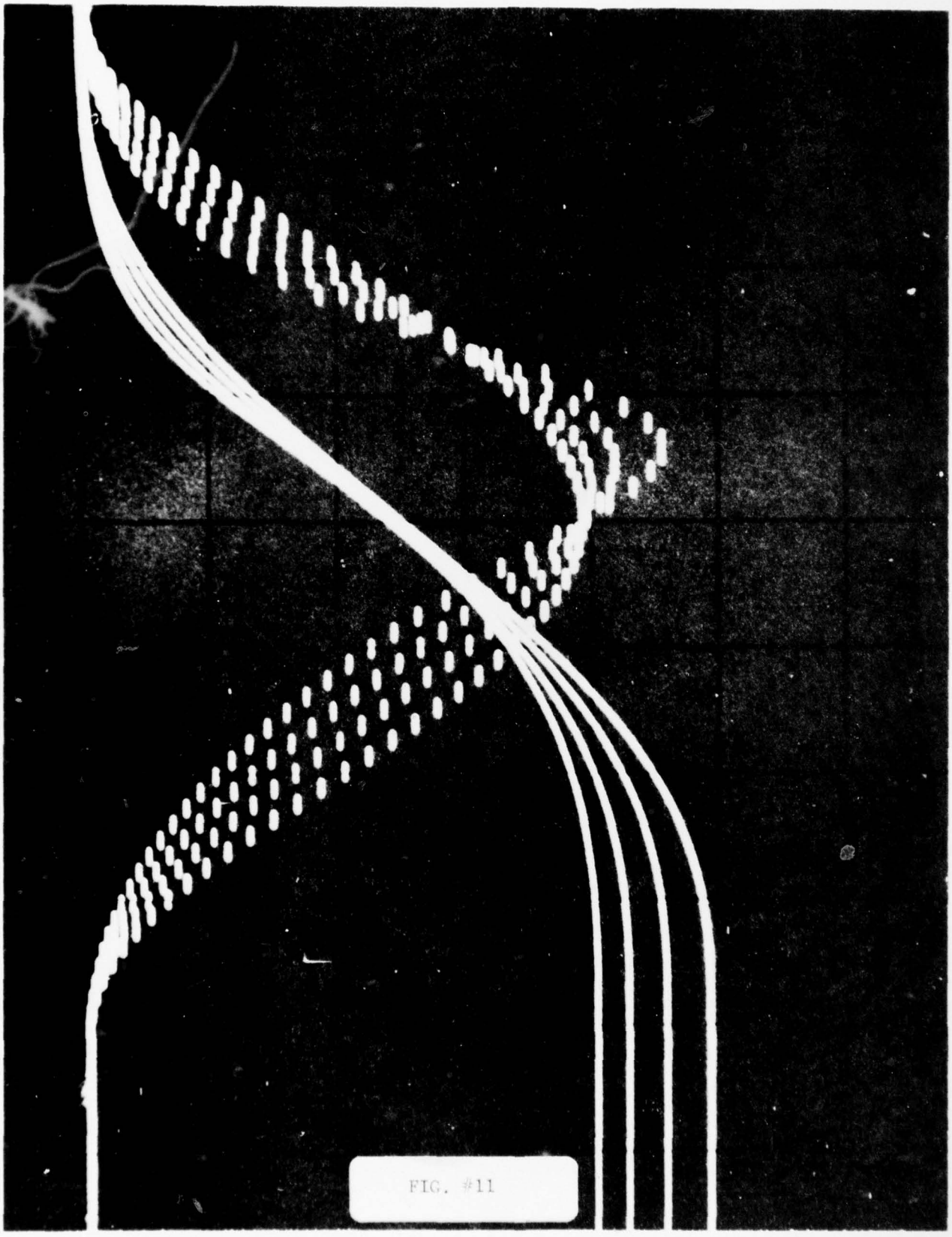

FIG. #11

FIG. #12

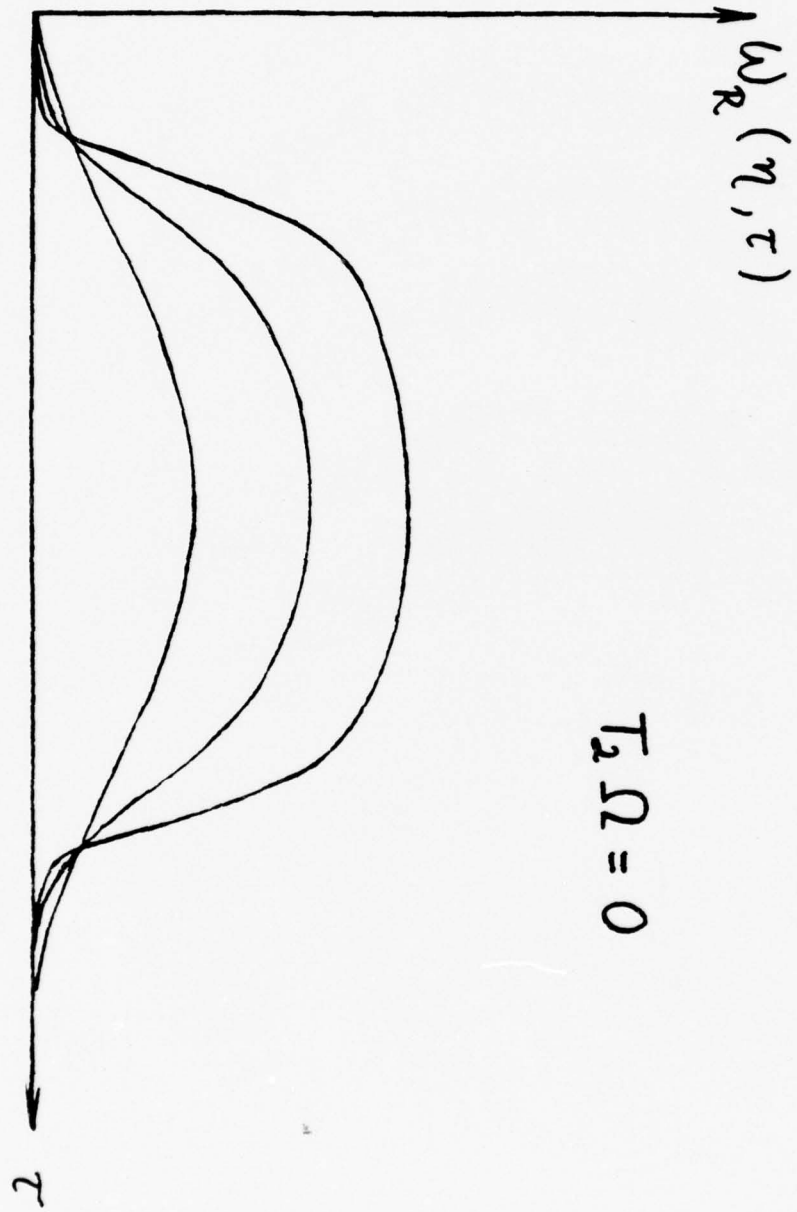

FIG. #13

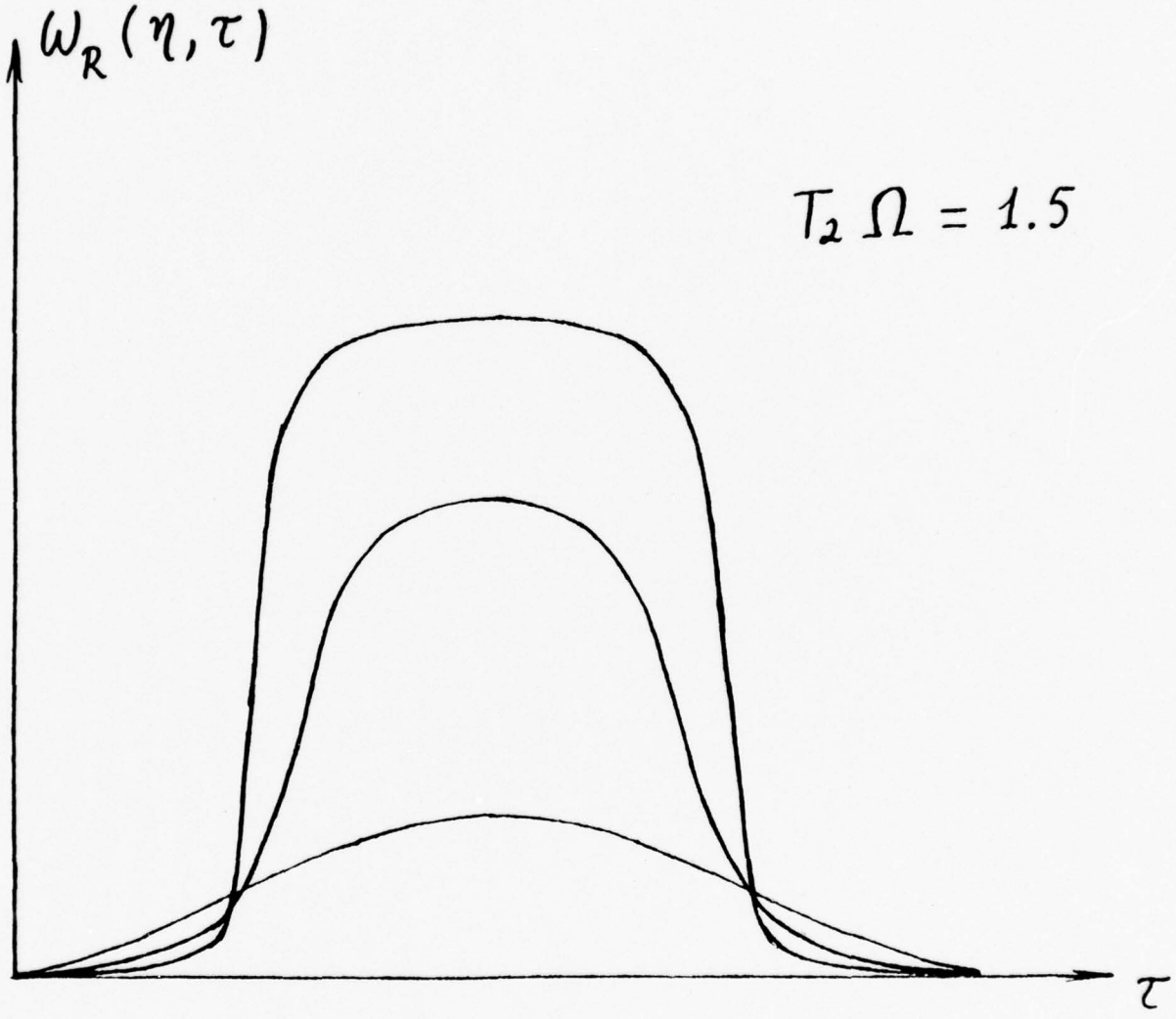

FIG. #14

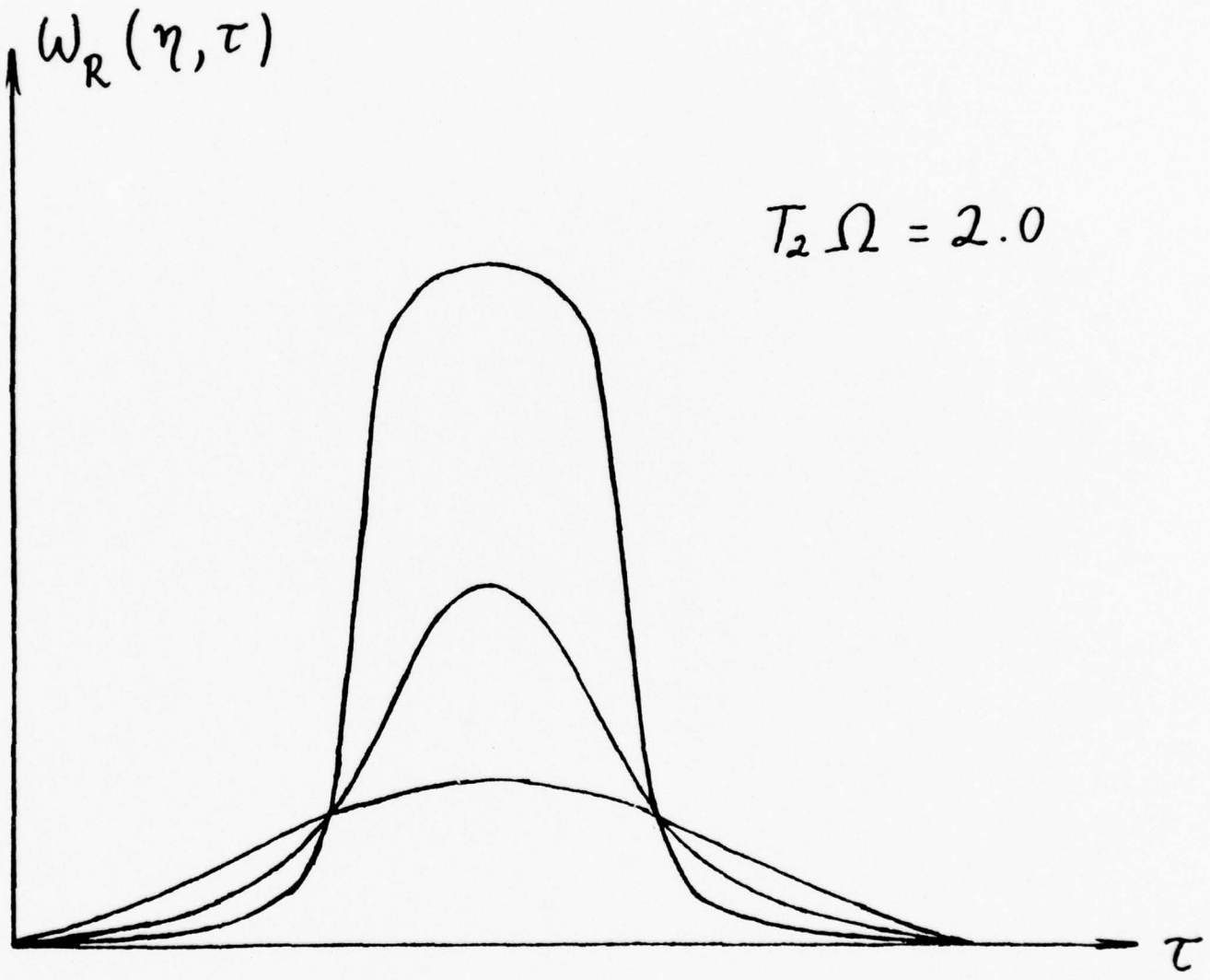

FIG. #15

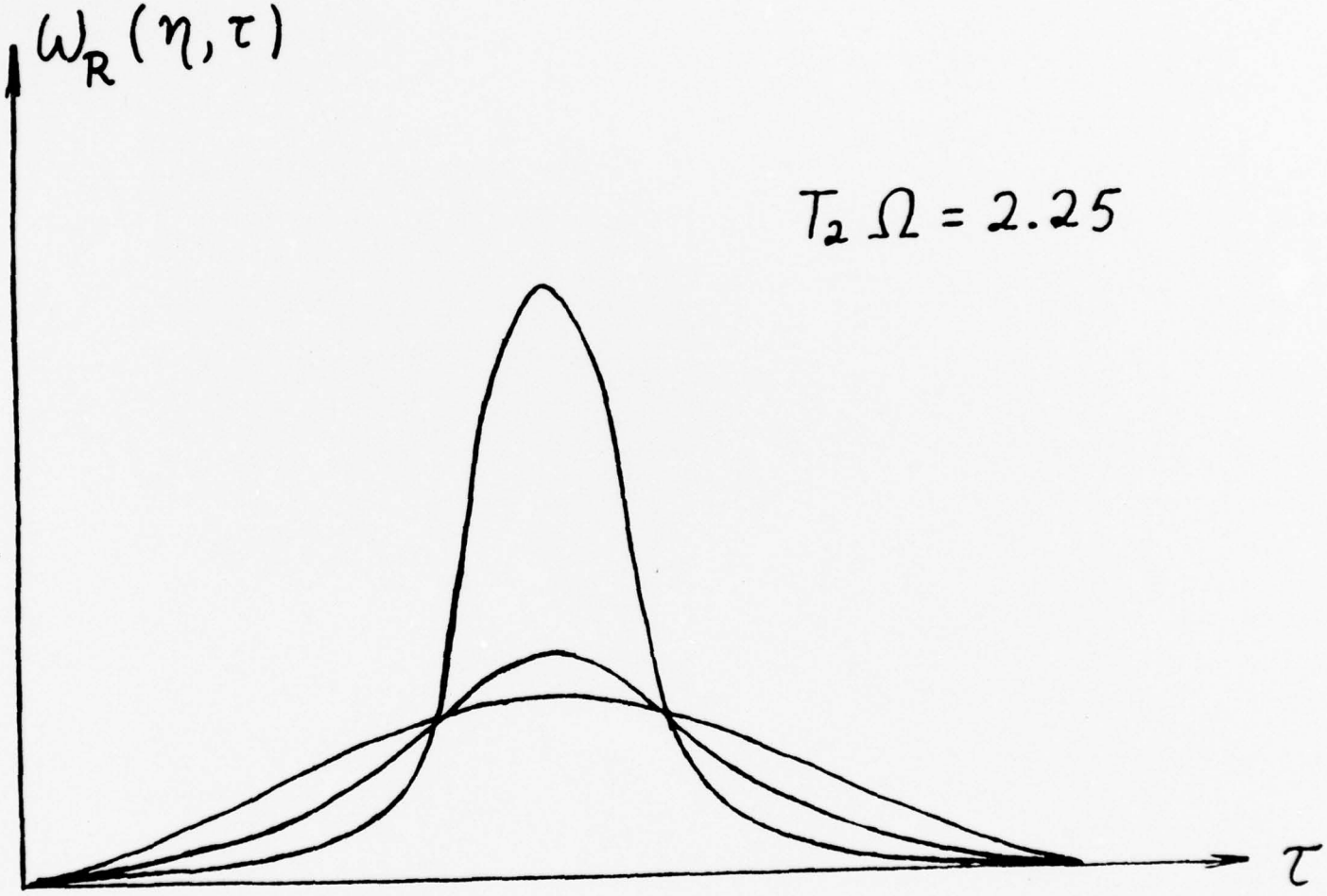

FIG. #16

FIG. #17

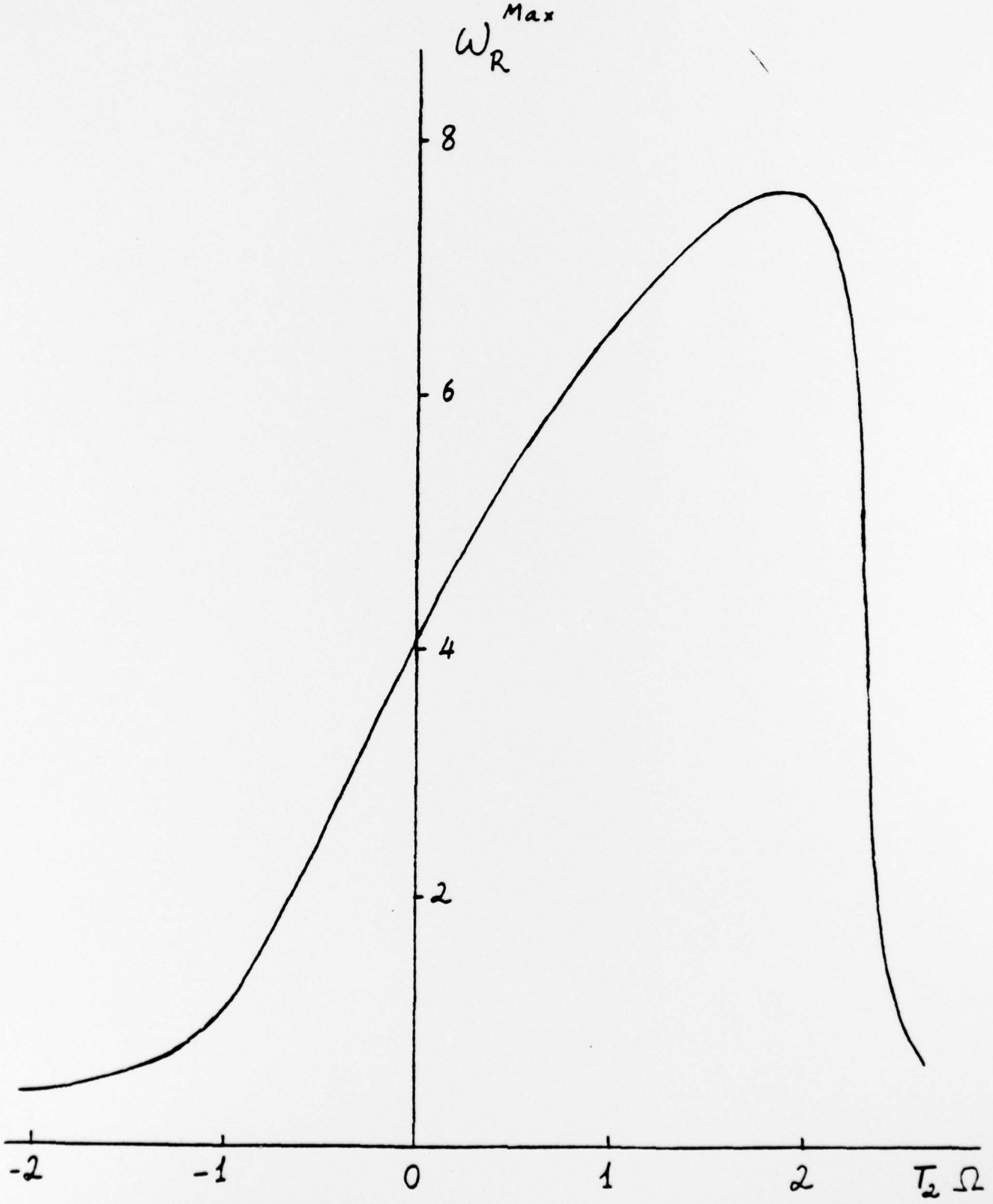

FIG. #18

Table 1

Figure number	Input area	G/ℓ	T_2/τ_p
3	3	2	12.5
4	3	2	1.25
5	3	2	0.38
6	8	2	12.5
7	9.8	5	∞
8	9.8	5	1.25
9	9.8	5	0.13
10	9.8	5	0.038
11	9.8	12	0.038

Table 2

Figure number	T_2	Γ	T_1/T_2	G/ℓ
12	-0.5	-0.7	2	5
13	0			
14	1.5			
15	2.0			
16	2.25			
17	2.5			

Figure Captions

1. Schematic energy level diagram for an active atom. The energy separation between the states $|a\rangle$ and $|b\rangle$ is approximately twice the energy of an incident photon. The symbol $|j\rangle$ collectively represents all the intermediate states.
2. The asymptotic steady state solutions of the area equation (3.9) correspond to the intercepts of the straight lines $\frac{\ell}{G}\,\Sigma(\eta)$ with the curve $1 - \cos\Sigma(\eta)$. The straight lines 1, 2 and 3 have slopes equal to 1, $\frac{1}{2}$ and 1/5 respectively. The stable solutions are marked with solid circles. The unstable solutions are marked with open circles. The critical slope (dashed line) is 0.7246.
3. Computer simulation illustrating the evolution of the pulse intensity through the amplifying medium. The different dashed curves represent the intensity envelope in different sections of the amplifier. The solid curves show the behavior of the corresponding integrated areas $\Sigma(\eta,\tau)$. The values of Σ at the far right give the total integrated area $\Sigma(\eta) = \lim_{\tau \to \infty} \Sigma$. The horizontal axis is the local time axis with $\tau = 0$ (leading edge of the pulse) at the far left. The input area is $\Sigma(0) = 3$ and the gain to loss ratio G/ℓ is 2. The value of T_2/τ_p is 12.5.
4. Same as Fig. 3 with $T_2/\tau_p = 1.25$
5. Same as Fig. 3 with $T_2/\tau_p = 0.38$
6. Evolution of the pulse intensity and pulse area corresponding to the initial value $\Sigma(0) = 8$, and to a gain to loss ratio of 5. The ratio T_2/τ_p is 12.5.
7. Pulse splitting and stable double-pulse propagation in the coherent limit. The input area is $\Sigma(0) = 9.8$ and the gain to loss ratio is 5. The ratio T_2/τ_p is 12.5.
8. Same as Fig. 7 with $T_2/\tau_p = 1.25$
9. Same as Fig. 7 with $T_2/\tau_p = 0.13$
10. Same as Fig. 7 with $T_2/\tau_p = 0.038$

11. Same as Fig. 10 with a larger gain to loss ratio ($G/\ell = 12$). The amplifier is now above threshold.

12. Computer simulation of the field transport equation (5.1) in the rate equation limit. The gain to loss ratio is equal to 5, the ratio T_1/T_2 equals 2, and the parameter Γ is taken to be -0.7 from an estimate based on spectroscopic data of Calcium atoms. The central portion of the input pulse is amplified. The leading and trailing edges are absorbed.

13. Same as Fig. 12 with the incident pulse in resonance with the active medium

14. Same as Fig. 13 with $T_2\Omega = 1.5$

15. Same as Fig. 13 with $T_2\Omega = 2.0$

16. Same as Fig. 13 with $T_2\Omega = 2.25$

17. Same as Fig. 13 with $T_2\Omega = 2.5$. The entire pulse is below threshold and no amplification occurs.

18. The maximum pulse intensity at the output of a fixed length of amplifier is plotted as a function of the detuning parameter $T_2\Omega$. The gain to loss ratio is 5. The ratio T_1/T_2 is 2 and the parameter Γ equals -0.7.

Table Caption

Table 1. Summary of the input data used for the hybrid computer simulation.

Table 2. Summary of the input data used for the computer simulation of the transport equation (5.1).

References

1. A.M. Prokhorov, Science, 149, 828 (1965)

2. P.P. Sorokin, N. Braslau, IBM J. Res. Dev. 8, 177 (1964).

3. S.R. Hartmann, IEEE J. Quant. Electron. QE-4, 802 (1968)

   E.M. Belenov, I.A. Poluektov, Sov. Phys. JETP 29, 754 (1969)

   M. Takatsuji, Phys. Rev. B2, 340 (1970), Ibid A4, 808 (1971)

   M. Takatsuji, Physica 51, 265 (1971)

   D. Grischkowski, Phys. Rev. Lett. 24, 866 (1970)

   N. Tan-no, K. Yokoto, H. Inaba, Phys. Rev. Lett. 29, 1211 (1972)

4. See for example D. Grischkowski, in Laser Applications to Optics and Spectroscopy, Vol. II of Physics of Quantum Electronics Series, Eds. S.F. Jacobs, M. Sargent III, J.F. Scott, M.O. Scully (Addison-Wesley 1975).

5. L.E. Estes, L.M. Narducci, B. Shammas, Lettere al Nuovo Cimento, Serie 2, 1, 175 (1971).

6. R.L. Carman, Phys. Rev. A12, 1048 (1975)

7. F.T. Arecchi, R. Bonifacio, IEEE J. Quant. Electron. QE-1, 169 (1965)

8. L. Allen and J.M. Eberly "Optical Resonance and Two-Level Atoms", Wiley, New York (1975), Chapter 2.

6. Measurement of the Two-Photon Absorption coefficient of ZnS

Our experimental effort has been directed to the measurement of the two-photon absorption coefficient of a sample of hexagonal ZnS with its optic axis aligned perpendicular to both the direction of propagation of the incident pulse and its direction of polarization.

Our measurements have been carried out with a Q-switched ruby laser as the source of radiation. The instrumental set-up is shown in Fig. 1. The pulsed output of the laser operating at a fixed pump power was passed through a 3 cm cell with plane parallel windows containing a dilute solution of copper sulphate. The cell was used as a variable attenuator with several advantages with respect to more conventional prism polarizers. We have found that the amount of attenuation can be controlled accurately and reproducibly by varying the concentration of copper sulphate. In addition, problems related to beam displacement which we experienced with prism polarizers in the intial phases of the work, were eliminated. The cell was fastened to a three-point kinematic mount. This device enabled us to remove the cell for cleaning and refilling and to reposition it accurately without further alignment.

After passing through a pair of apertures, 3.5 mm. in diameter, 10% of the incident beam was reflected by a glass beam splitter placed at an angle of 30° from the beam direction. The reflected beam was monitored by an EG&G S-100 photodiode at a distance of 3 m. from the beam splitter. A series of apertures and two pieces of ground glass were placed in front of the detector to attenuate the beam and to average inhomogeneities in the beam tranverse profile.

The transmitted portion of the beam was propagated through the hexagonal ZnS crystal sample having a length of 0.84 cm. The crystal was also fastened to a three-point kinematic mount so as to be removable during the calibration

procedure and repositioned with good accuracy for the final measurements.

The laser pulse transmitted through the crystal was detected by a photodiode identical to the one used for monitoring of the incident beam. The output signal from the second photodiode was delayed through a 150 μsec delay line, and added to the signal from the input detector. Both signals were displayed on the same channel of an oscilloscope (Tektronic model 7603).

The data collection was based on the measurement of the peak voltages produced by the incident and transmitted pulses.

The two-photon absorption coefficient α for a medium of given thickness ℓ, linear absorption coefficient β, and reflectively R can be arrived at from the measurement of the incident and transmitted intensities I_o and I. The intensities are related to one another by the well known expression

$$I = \frac{(1-R)^2 I_o e^{-\beta \ell}}{1 + (1-R) e^{-\beta \ell} \alpha \ell I_o} \quad . \tag{6-1}$$

Our measurements are based on the observation of the output voltages from the two photodiodes. We have checked the response of the detectors over the range of intensities of interest in this work, and established that the voltages V_1 and V_2 from the two photodiodes can be accurately expressed in terms of the incident and transmitted intensities by the relations

$$V_1 = a I_o \quad , \quad V_2 = b I \tag{6-2}$$

where a and b are constants depending on the geometry of the set-up and on the sensitivity of the diodes. In terms of the measured voltages eq. (6-1) can be cast into the form

$$\frac{a'}{b'} \frac{V_1}{V_2} = 1 + a' \alpha \ell V_1 \quad , \tag{6-3}$$

where

$$a' = (1-R)\, e^{-\beta \ell}\, a \quad ,$$
$$b' = \frac{b}{1-R} \quad . \tag{6-4}$$

The parameter a was determined by removing the crystal and measuring the total energy of a series of pulses with a calibrated thermopile. Because of the low amount of impurities and of scattering losses in the crystal, we felt justified in neglecting the single photon absorption contribution. The Fresnel reflection coefficient was calculated from the known index of refraction of the crystal at 7000 Å. For normal incidence we found $R = 0.04$. Finally the quantity a' was related to the measured value of a by

$$a' = 0.96\, a$$

The rate a'/b' was extrapolated from the data by using the limiting constraint

$$\lim_{I_o \to o} \frac{a'}{b'} \frac{h_1}{h_2} = 1 \tag{6-5}$$

The results of our measurements, following the data reduction outlined above, are shown in Fig. 2. A least square fit of the data to the theoretical relation

$$\frac{I_o}{I} = 1 + \alpha \ell\, I \tag{6-6}$$

has lead to the experimental two-photon absorption coefficient $\alpha = 0.013$ cm/MW.

Considering the indirect nature of the measurement (only one of the detectors was calibrated to measure absolute power) and the lack of direct information on the linear absorption coefficient, our confidence in the measured value is only to within a factor of 2. Our method however is rather simple to use and susceptible of improvements. For example it would have been desirable to switch the detectors and to repeat the same sequence of measurements.

Assitional data are being collected at this time by Professor Tuft at Worcester Polytechnic Institute.

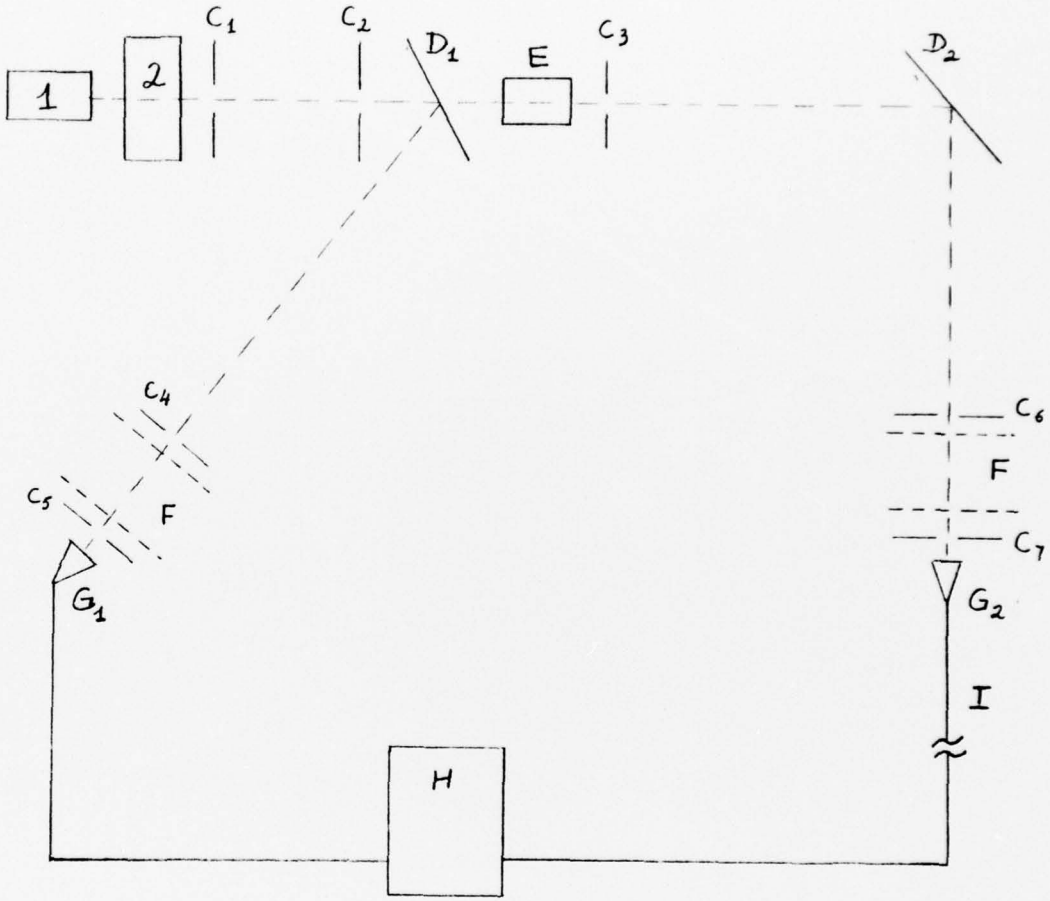

Fig 1.

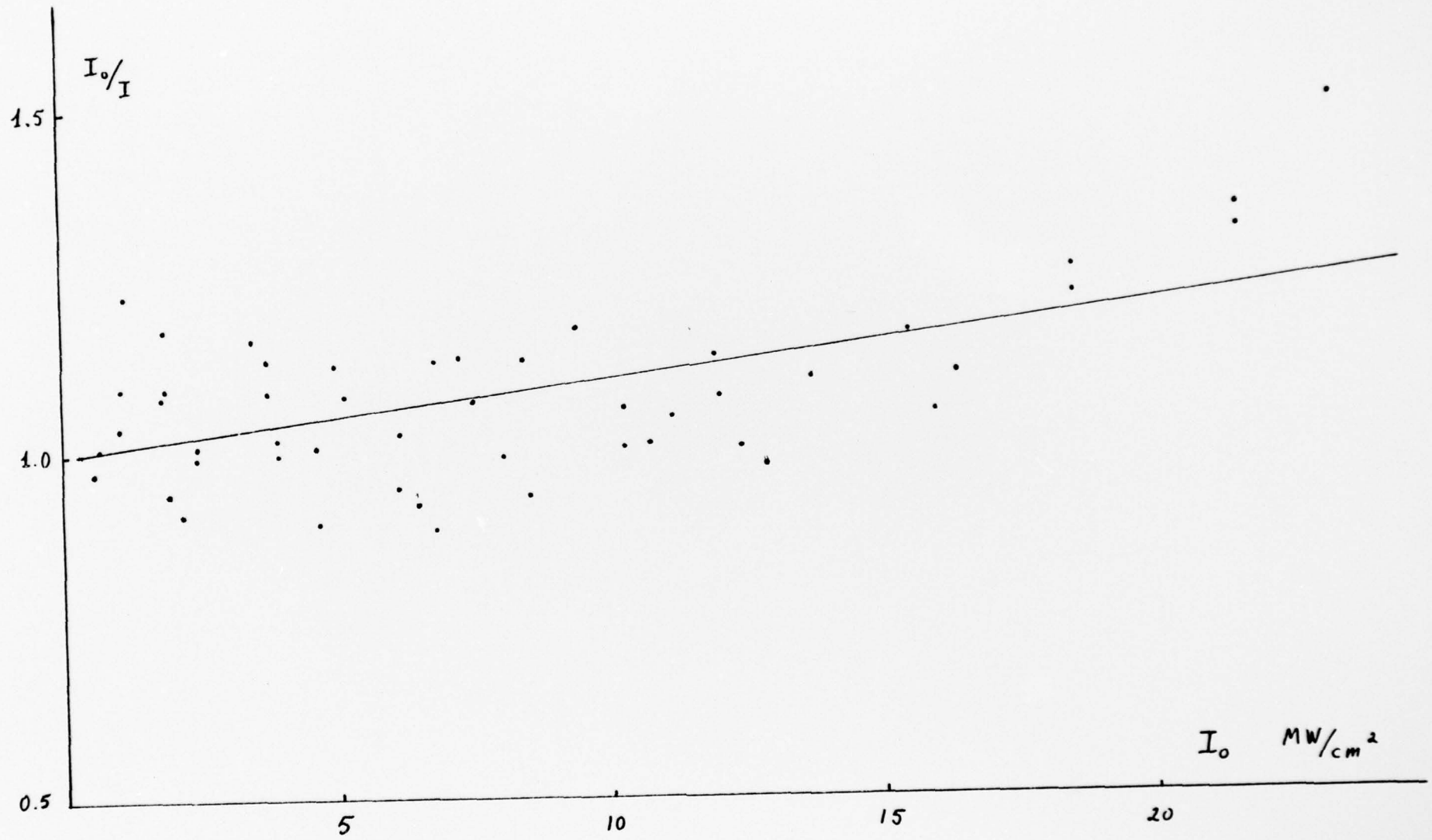

Fig. 2

FIGURE CAPTIONS

Fig. 1. Experimental set-up for the measurement of the two-photon absorption coefficient of ZnS at the ruby laser operating wavelength 6943Å.

1 Ruby laser

2 Cupper Sulphate cell

C_{1-7} circular apertures

D_1, D_2 beam splitters

E ZnS crystal

F ground glass diffusers

G_1, G_2 photodiodes

H Oscilloscope

I 150 μsec delay line

Fig. 2. Experimental points after the data reduction process described in the text showing the behavior of the ratio I_o/I as a function of the incidence pulse intensity. The solid line is the result of the least square fit of the data points to Eq. (6.6). The measured two-photon absorption coefficient in ZnS is $\alpha = 0.013$ cm/MW.